

**DESIGN AND USABILITY OF A SYSTEM FOR THE STUDY OF
HEAD ORIENTATION**

A Thesis
Submitted to
the Temple University Graduate Board

In Partial Fulfillment
of the Requirements for the Degree
MASTER OF SCIENCE
in **ENGINEERING**

by
Ji Chen
May, 2010

Thesis Approval:

Kurosh Darvish, Thesis Advisor, Department of Mechanical Engineering

William G. Wright, Department of Physical Therapy

Emily A. Keshner, Department of Physical Therapy

Dmitri Vainchtein, Department of Mechanical Engineering

ABSTRACT

Design and Usability of a System for the Study of Head Orientation

Ji Chen

Master of Science in Engineering

Temple University, May 2010

Kurosh Darvish

The ability to control head orientation relative to the body is a multi-sensory process that mainly depends on three sensory pathways namely, proprioceptive, vestibular, and visual. A system to study the sensory integration of head orientation was developed and tested. A test seat with five-point harness was assembled to provide the passive postural support. A light-weight head-mount display (HMD) was designed for mounting multi-axis accelerometers and a mini- CCD camera to provide the visual input to virtual reality (VR) goggles with 39° horizontal field of view. A digitally generated sinusoidal signal was delivered to a motor-driven computer-controlled sled on a 6m linear railing system. A data acquisition system was designed to collect acceleration data. A pilot study was conducted to test the system. Four young healthy subjects were seated with their trunks fixed to the seat. Subjects received a sinusoidal anterior-posterior translation with peak acceleration of 0.06g at 0.1Hz and 0.12g at 0.2Hz, 0.5Hz and 1.1Hz. Four sets of visual conditions were randomly presented along with the translation. These conditions included eyes open looking forward, backward, and sideways, and also eyes closed. Linear acceleration data were collected from linear accelerometers placed on the head, trunk and seat and were processed using Matlab. The head motion was analyzed using Fast Fourier Transform (FFT) to derive gain and phase of head pitch acceleration relative to seat linear

acceleration. A randomization test for two independent variables was used to test significance of visual and inertial effects on response gain and phase shifts. Results show that the gain was close to one with no significant difference among visual conditions across frequencies. The phase was shown to be dependent on the head strategy each subject used.

ACKNOWLEDGEMENT

First I would like to thank my primary advisor Professor Kurosh Darvish who gave me the opportunity and a financial support to do my master degree's thesis on the postural control related research. Many thanks also go to my three other advisors: Professor William G. Wright, Professor Emily A. Keshner and Professor Dmitri Vainchtein. Your guidance and patience takes me to finish the thesis. The experience would definitely be appreciated for the rest of my life. I would like to thank people who became subjects for the research: Vasily Romanov, Sahand Hariri Akbari, Keith Shaffer, Peter Strahs. I would also feel grateful to my colleagues at Temple Biomechanics Laboratory and from other laboratories for their support: Mehdi Shafieian, Kaveh Laksari, Cristina Parenti, Vasily Romanov, Sahand Hariri Akbari, Luis Breziner, Run Chang Ren. I feel indebted to Professor Vallorie Peridier whose faith and encouragement to me helps me explore my abilities. Special thanks are to ANALOG DEVICES for offering accelerometers and A/D convertors, and to MacPherson Control Products and National Instruments for the technical support to the research. .

TABLE OF CONTENTS

ABSTRACT.....	ii
ACKNOWLEDGEMENT	iv
TABLE OF CONTENTS.....	v
LIST OF FIGURES	vii
LIST OF TABLES	viii
CHAPTER 1 INTRODUCTION.....	1
CHAPTER 2 SYSTEM DEVELOPMENT.....	4
Overview.....	4
2.1 Seating System.....	4
2.2 Motion Stimuli.....	7
2.3 Visual Stimuli	15
2.4 Data Collection and Processing	16
2.4.1 Accelerometer	16
2.4.2 Motion tracking system.....	20
2.4.3 Data Processing.....	22
CHAPTER 3 PILOT STUDY	26
3.1 Study concerns	26
3.1 Subjects	27
3.2 Design of Experiment (DOE)	28
CHAPTER 4 RESULTS	33
CHAPTER 5 DISCUSSION	45
CHAPTER 6 CONCLUSION	48
REFERENCES	49

APPENDIX A	HEAD COORDINATION WITH MOTOR-NEURON DISEASES DURING A-P TRANSLATION.....	52
APPENDIX B	ACCELERATION CONVERSION FACTOR.....	59
APPENDIX C	MATLAB CODES FOR PROCESSING ACCLERATION DATA	61
APPENDIX D	RAW ACCELERATION DATA	66

LIST OF FIGURES

FIGURE 1-1 SENSORY AND MOTOR SYSTEMS CONTRIBUTED TO ORIENTATION IN SPACE (CLEMENT 2005).	1
FIGURE 2-1 SEATING SYSTEM CONFIGURATION.....	5
FIGURE 2-2 LINEAR TRANSLATION PROFILE	7
FIGURE 2-3 WH120 LINEAR RAILING SYSTEM (A) MH8500 SERVO MOTOR (B) THE LINEAR TRACK	9
FIGURE 2-4 (A) DRIVE MODULE OPERATIONS AND FEATURES (B) ANALOG COMMAND, SINGLE ENDED WIRING DIAGRAM	10
FIGURE 2-5 GENERATION OF SINUSOIDAL MOTION	11
FIGURE 2-6 LINEAR ACCELERATION AT 0.1Hz WITH INITIAL OVERSHOOT.....	12
FIGURE 2-7 A LINEAR ACCELERATION AT 0.1Hz WITH REMOVED OVERSHOOT.....	13
FIGURE 2-8 FRONTAL PANEL OF LABVIEW PROGRAM TO GENERATE THE SINUSOIDAL SIGNAL.....	14
FIGURE 2-9 CONFIGURATION OF AMPLITUDE OF CARRIAGE MOVEMENT.....	15
FIGURE 2-10 (A) A HELMET WITH A GIMBALED MINI-CAMERA MOUNTED ON THE TOP. (B) VIRTUAL	16
FIGURE 2-11 ADXL320EB AND ADXL321EB. LEFT IS THE SCHEMATIC DIAGRAM. RIGHT IS THE REAL PRODUCT.	18
FIGURE 2-12 FOUR-POINT TUMBLE TEST FOR X DIRECTION.....	19
FIGURE 2-13 ACCELERATION CALIBRATING CIRCUIT	19
FIGURE 2-14 PHANTOM CAMERA LAYOUT.....	22
FIGURE 2-15 THE SCHEME OF PROCESSING ACCELERATION DATA	23
FIGURE 2-16 RIGHT-HAND ROTATION OF HEAD ABOUT Y AXIS BY AN ANGLE θ	24
FIGURE 2-17 IMAGE PROCESSING MOTION OF THE HEAD AND SEAT.	26
FIGURE 3-1 ACCELERATION DATA COLLECTION	27
FIGURE 3-2 ORIENTATION OF ACCELEROMETERS ON HMD.....	32
FIGURE 3-3 CXM544 ORIENTATION SENSOR.....	32
FIGURE 4-1 ACCELERATION OF THE HEAD, TRUNK AND SLED WITH SW AT 0.5Hz.....	33
FIGURE 4-2 ACCELERATION PROCESSED BY FITTED-SINE MODEL WITH SW AT 0.5Hz.....	34
FIGURE 4-3 FREQUENCY SPECTRUM OF ACCELERATION AT 0.5Hz AND SW	35
FIGURE 4-4 HEAD PITCH ACCELERATIONS AND CORRESPONDING ACCELERATION OF THE SLED AND TRUNK WITH SW AT 0.5Hz.	36
FIGURE 4-5 GAINS OF HEAD ACROSS FREQUENCIES IN EACH VISUAL CONDITION.....	38
FIGURE 4-6 PHASE OF HEAD ACCELERATION RELATIVE TO SLED.....	39
FIGURE 4-7 POLAR PLOTS OF GAIN AND PHASE OF HEAD MOTION (A) AT 0.1Hz (B) 0.2Hz.....	41
FIGURE 4-8 POLAR PLOTS OF GAIN AND PHASE OF HEAD MOTION (A) AT 0.5Hz (B) 1.1Hz.....	42
FIGURE 4-9 THE AVERAGED GAIN OF HEAD PITCH ACCELERATION WITH RESPECT TO FREQUENCIES OF THE MOTION STIMULI	43
FIGURE 4-10 THE AVERAGED GAIN OF HEAD PITCH ACCELERATION WITH RESPECT TO VISUAL CONDITION.....	44
APPENDIX A-1 ACCELERATION OF THE HEAD, TRUNK AND SLED DURING THE FIRST-TRIAL LINEAR	53
APPENDIX A-2 FREQUENCY SPECTRUM OF ACCELERATION AT 0.6Hz WHEN EYES WERE CLOSE	54
APPENDIX A-3 GAINS OF HEAD ACROSS FREQUENCIES IN EACH VISUAL CONDITION.	57
APPENDIX A-4 PHASE OF HEAD ACCELERATION RELATIVE TO SLED	53

LIST OF TABLES

TABLE 1 PHYSICAL CHARACTERISTICS OF SUBJECTS (THE # REPRESENTS THE SUBJECT NUMBER).....	28
TABLE 2 CONFIGURATION OF MOTION STIMULI	28
TABLE 3 EXPERIMENTAL MATRIX.....	30
TABLE 4 THE SIGNIFICANCE OF FREQUENCIES AND VISUAL CONDITIONS AND THE INTERACTION BETWEEN THEM	44
TABLE 5 CONFIGURATION OF SLED ACCELERATION.....	52
TABLE 6 SUBJECT 1	66
TABLE 7 SUBJECT 2	67
TABLE 8 SUBJECT 3	69
TABLE 9 SUBJECT 4.....	70

CHAPTER 1

INTRODUCTION

Postural orientation is a multi-sensory process which is mainly attributed to three sensory systems: visual, vestibular, and proprioceptive systems (Keshner and Peterson 1995) (Figure1-1). Falls resulting in postural instability have become a big health concern. According to the Centers for Disease Control and Prevention (CDC), falls are a leading cause of death related to injury in the United States. More than one third of adults aged 65 and older fall every year in the US. Children aged 14 and under account for one third of all fall-related visits to hospital emergency room. The treatment for these fall-related injuries is very costly since it often includes hospitalization and as well as long-term care after discharge. (Alexander *et al.* 1992). In 2000, the total direct cost of all fall injuries for people 65 and older exceeded \$19 billion. (Stevens *et. al* 2006)

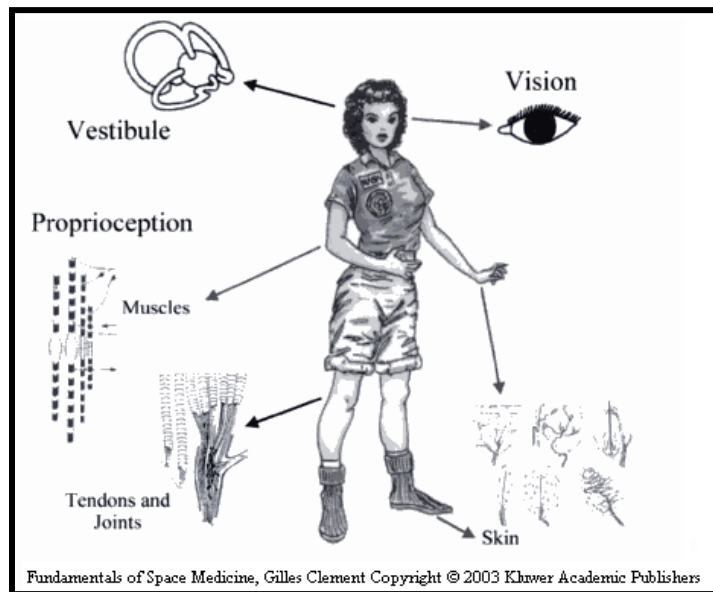


Figure 1-1 sensory and motor systems contributed to orientation in space (Clement 2005). The eyes, the inner ear and proprioceptors in the skin, muscles and joints all participate in maintaining balance.

Investigations of postural orientation have looked into many factors that affect one's postural stability. Some of these factors include: the role of visual context, the dynamic or static state of a subject, the postural state of the subject (sit or stand), the effect of passive versus self-generated movement, rotational versus translational movement (Wright and Glasauer 2006). Considerable attention has been directed toward understanding how our visual, vestibular and proprioceptive systems, as both individual and combined variables, are utilized to orient ourselves. Furthermore, many disorders of movement, such as stroke, Parkinson's disease and Huntington's disease, have been investigated to explore possible countermeasures to rehabilitate postural instability.

The head and neck sensorimotor system is a good prototype for the study of whole body postural. (Darvish *et al.* 2008) All three of the sensory systems are integrated in the central nervous system (CNS) for this multi-joint system. Thus, as part of a plan to develop a laboratory to explore multimodal control of head orientation in space, a system was designed for investigating how vestibular/proprioceptive inputs integrate with visual input to control the head stabilization.

In a preliminary study of subjects with two motor-neuron diseases, the gain and phase of pitch acceleration of the head related to linear acceleration of the sled was used as two dependent variables to study the dynamics of head motion to linear acceleration of the sled in a patient population (Appendix A). The outcome of gain analysis indicates that the gain has no significant difference between eyes open and eyes closed and between two

diseases across three frequency points (0.6Hz, 0.8Hz, 1.11Hz). The result of phase response suggests that patient subjects used neck-locked strategy to control the head motion. To obtain the insight of head control for normal subjects in similar setting, primary aims of my master degree's thesis were to create the mismatched sensory inputs during passive accelerations of the body and to examine kinematic data such as displacement and acceleration. Along with the system, an experimental paradigm was designed and a pilot study was performed. Codes written in Matlab were used to process the acceleration data. The high-speed camera along with markers recorded the displacement of head and sled motion. Vision Assistance software was used to process the displacement data. Gains and phase shifts of head pitch acceleration with respect to trunk were calculated. A nonparametric test was applied to study the effect of visual inputs and frequency of physical stimuli on the gains and phase shifts.

CHAPTER 2

SYSTEM DEVELOPMENT

Overview

The system can be divided into four parts: seating system, motion stimuli, visual stimuli, data collection and processing. Seating system allowed subjects to be seated with their trunk fixed and their head free to move. Motion and visual stimuli produce inertial and visual inputs to sensory systems of subjects respectively. By aligning motion with visual inputs concordantly or discordantly, matched or mismatched sensory feedback could be created. Linear acceleration of the head, trunk and sled, and displacement of the head and sled were collected when subjects were exposed to motion and visual stimuli. Each channel of acceleration data were sorted out and processed by a linear regression model to find its magnitude, phase and offset. Each channel of displacement data were processed by the Vision Assistance software.

2.1 Seating System

The seating system provided the place to house the subject (Figure 2-1). It consists of a standard race-car seat, five-point harness belts, a pair of feet straps, a cubic frame and a plate platform. During the test, chest and limbs were expected to be restrained to the seat and the head and neck to be able to move freely. The seat was also expected to provide a good comfort to the subject. We chose a CORBEAU fixed back seat. It has a bolster support. The ultimate lateral support with well-defined thigh, knee, and shoulder bolsters, allowed the subject to remain in the optimal seating position. It has harness slots for 5-

point harness capability. A submarine slot was already installed for a 5th strap. A couple of ploymer foam were placed between the seat and the subject to creat the space for the head and neck to move.

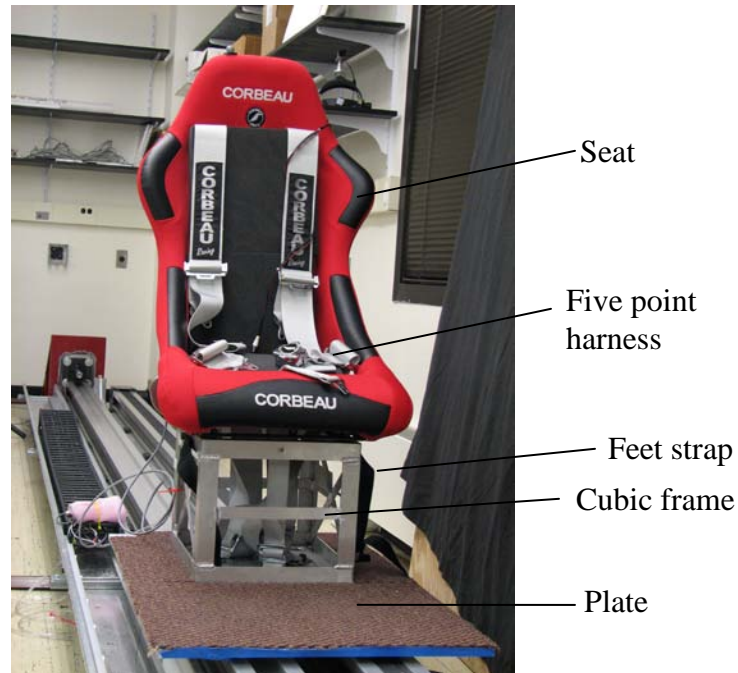


Figure 2-1 Seating system configuration

Five-point harness was used to restrian the torso movment. It has a bolt-in feature. End of the straps are equipped with a bolt, which allowed us to connect them to the linear track. Wrap-around option allowed us to wrap the two rear straps around a harness bar. Length adjusters of belts could restrain subjects with different size. To secure substantial restriction of motion detection by proprioceptive receptors from lower limbs and as well as safety concern, we also used an extra pluggable strap to restrain the feet during the test.

A cubic frame (14.25"×13.5"×12") and an aluminum plate (36"×24") provided the connection between the seat and linear track. The reliability of frame was analyzed. We assumed the maximum load F

$$F = W_1 + W_2 = 230 + 50 = 280 \text{ lbs} \quad (1)$$

Where

- W_1 represents the subject weight; W_2 represents the total weight of seat and five point harness.

The load on each corner was therefore 70 lbs. Given the length and the width of frame was very close, the load was considered evenly placed on each side. The load would mainly cause the compression of frame. The direction of load is transverse to the direction of motion. Therefore the shear stress is mainly our concern. The formula for shear stress τ in a direct shear:

$$\tau = \frac{V}{A} \quad (2)$$

Where:

V = shear force at that location, measured in Newton's.

A = area of section parallel with shear force, measured in square meters.

The cross-sectional area A is 0.375 inch². So the shear stress is:

$$\tau = 70 / 0.375 \approx 186.67 \times 6894.76 \text{ Pa} \approx 1.29 \text{ MPa} \quad (3)$$

The general yield strength of aluminum is 400 Mpa. The theoretical shear stress is far less than the yield strength. We could say that the design of cubic frame is reliable in both static and slow-motion conditions. Furthermore, the linear track can support dynamic

5000N load in the longitude axis. The amount is much bigger than the total weight of subject and seating system ($\leq 500N$). As a result, we believe that the linear track and servo motor wouldn't be damaged during the translation.

2.2 Motion Stimuli

A motion system was developed to create the linear translation (Figure 2-2). A linear translation or sinusoidal motion profile allows for spatiotemporal dynamics to be dissociated between velocity-sensitive visual detectors and acceleration-sensitive inertial detectors, and thus can provide insight into how visual and vestibular/proprioceptive sensory systems are integrated in a virtual environment. (Wright and Schneider 2009)

Requirements for the translation are listed as follows:

- 1) A sinusoidal motion has adjustable frequencies.
- 2) The displacement of motion is adjustable.
- 3) The running cycle of motion is controllable.

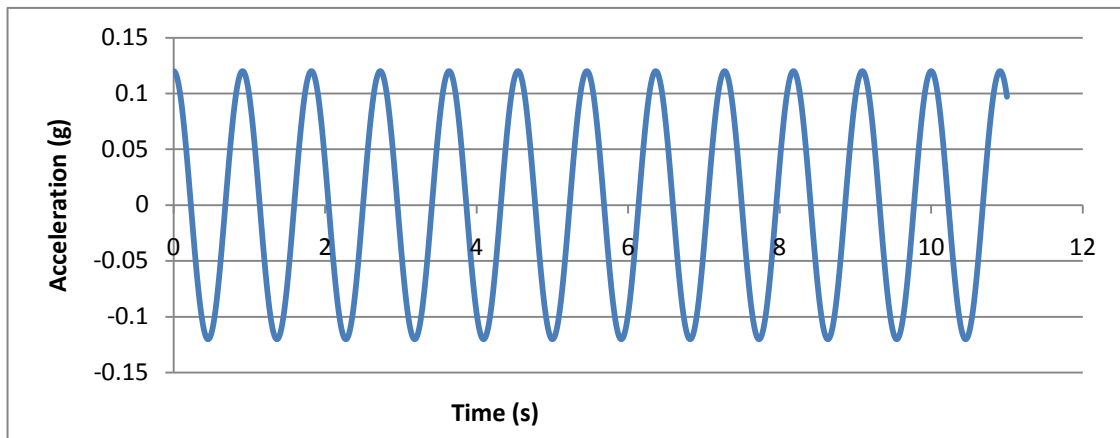


Figure 2-2 linear translation profile

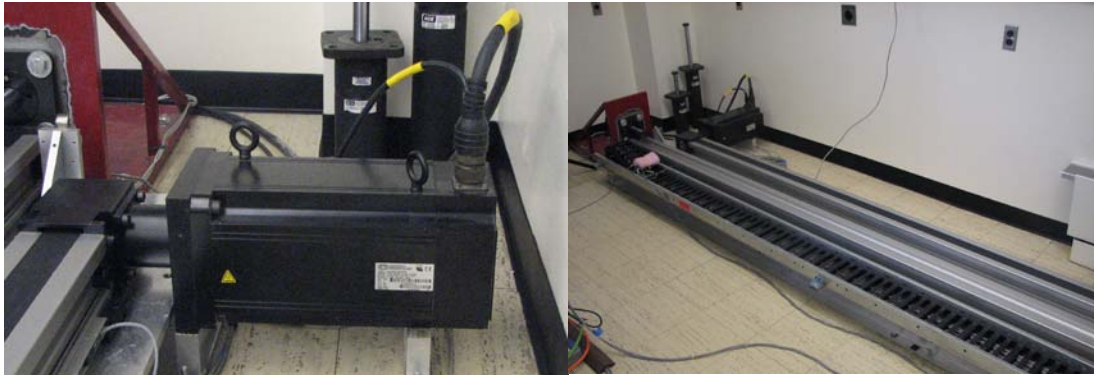
The approach to generate the translation was first to program a sinusoidal signal in computer, and then to export the signal from a computer interface, finally to use the

signal to control the motor that physically performs the linear translation. Along with concerns of accurate control and synchronization, a LabVIEW program implements a Data Acquisition (DAQ) card (NI-PCI 6281, National Inst.) to produce the sinusoidal signal and control its parameters such as frequency, amplitude, time-length, and triggering.

Signals were physically obtained from NI-PCI 6281 and then filtered through a NI signal conditioning system (SC-2311, National Inst.). SC2311 has a breaking board and can accommodate up to 8 pluggable 5B analog modules. The breaking board has two analog-output channels DAC0 and DAC1. The signal-ended voltage output from the DAQ card is transmitted by a shielded cable to output channels on the board. 5V DC on-board voltage supply and triggering channels (such as PFI0, PFI1, PFI2) create the interface for synchronizing the voltage output with the data acquisition system and a high-speed camera. 5B analog modules provide a signal conditioning solution for data acquisition.

Sinusoidal signals were sent to the Modular Drive System (MDS). RS-232 Serial Connector provides the I/O communication interface between MDS and PowerTools 5.0 software. The Windows® based software PowerTools 5.0 was used to adjust motor parameters of a linear railing system WH120 (WIESEL™ SPEEDLine®). The motor is geared up to tracks of WH120 whose carriages perform the linear translation (Figure 2-3). The railing system consists of two 6m parallel tracks, one is active and transfers the rotation of the motor to the linear motion by a rubber band, and one is passive, with a

freely sliding carriage that can move with the active carriage by bolting them together (Darvish 2009).

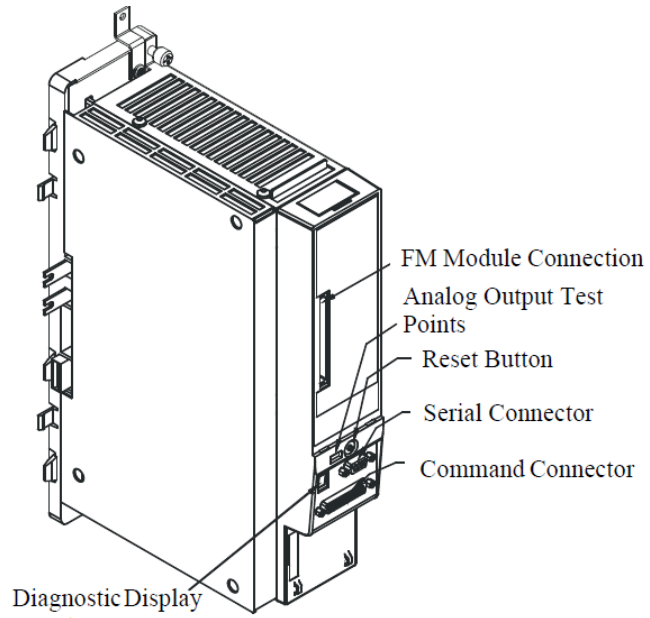


(a)

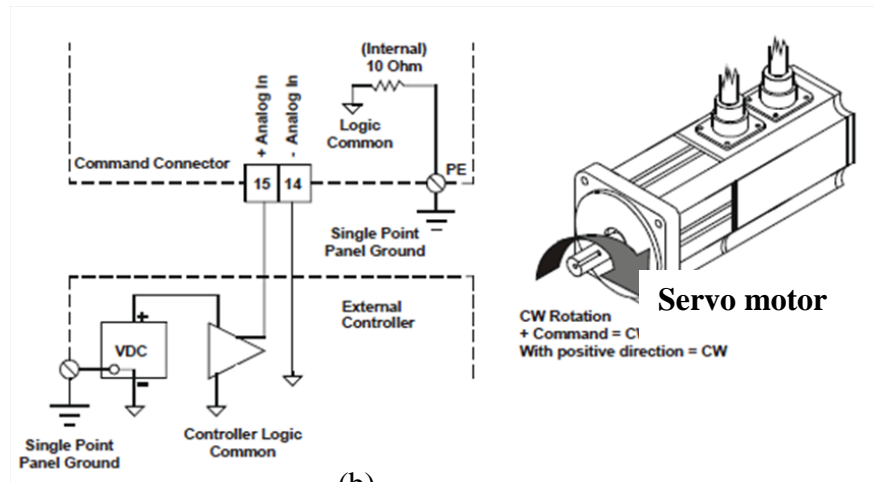
(b)

Figure 2-3 WH120 linear railing system (a) MH8500 servo motor (b) the linear track

MDS has connections for digital I/O, analog I/O, encoder feedback and the ability to connect FM modules for more functionality (Figure 2-4a). Command Connector (J5) in MDS was used as the I/O interface to receive external analog signals. Pin 14 and 15 in the J5 connector were physically connected through a cable with a 44-pin D-sub connector to receive the sinusoidal signal. The single-ended sinusoidal signal from these two pins was transformed by MDS to drive the servo motor (Figure 2-4b).



(a)



(b)

Figure 2-4 (a) Drive Module Operations and Features (b) Analog Command, Single Ended Wiring Diagram

The procedure of generating linear translation is described in Figure 2-5.

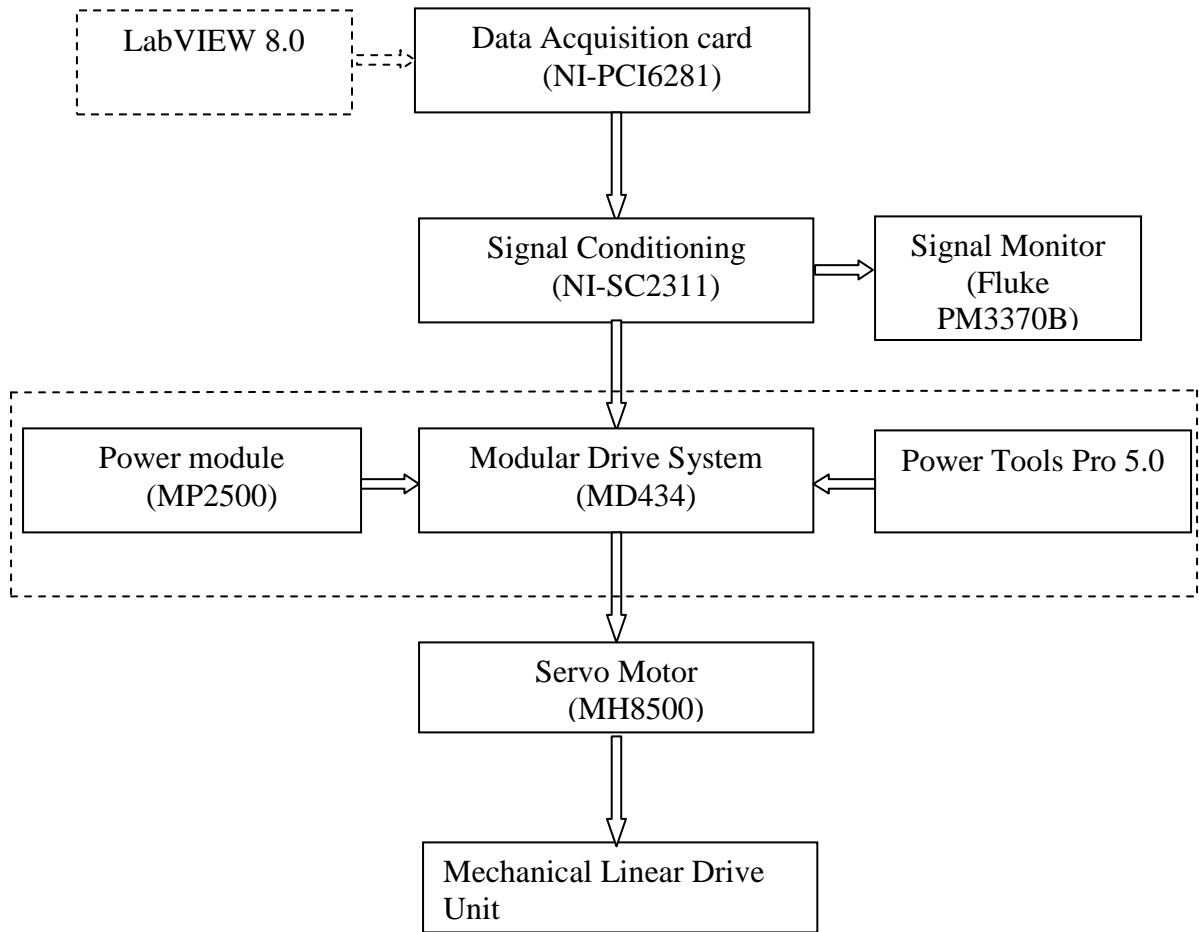


Figure 2-5 Generation of sinusoidal motion

One technical constraint with generating the translation is that the acceleration had to undergo an instantaneous change at the very beginning of each trial. This is due to the initial conflict between the velocity of translation and its displacement. Both the displacement and velocity set out from zero. But according to the Newton’s second law for the motion system the velocity would be at its maximum value when the displacement is zero. Hence the velocity has to reach its maximum in a very short time. The sudden change of velocity causes the initial acceleration jump. The high maximum velocity especially at 0.1Hz and 0.2Hz, leads to the acceleration “overshoot” (Figure 2-6). Just

like noise in the electrical signal, initial jumps caused a big disturbance to sensory systems of test subjects in initial conditions. Because the peak acceleration of initial jumps was much higher than the peak acceleration we expected from the translation. As a consequence, the head movement would be affected and sensory systems would react and adapt to these jumps differently for each frequency, which makes it difficult to determine the real response of head to the translation. Therefore although it is impossible to remove these jumps completely, it is necessary to reduce them to the level below the maximum acceleration and preferably make them relatively equal across conditions.

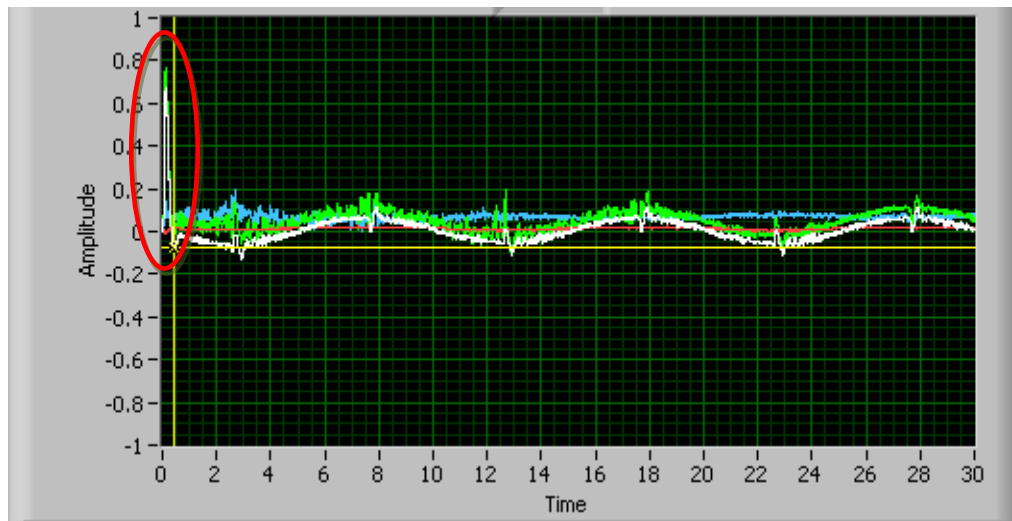


Figure 2-6 linear acceleration at 0.1Hz with initial overshoot. White and Green sine waves represent the linear translation of test seat measured from two accelerometers respectively. Red circle highlights initial overshoot of acceleration.

To reduce the jump, the carriage was programmed to let the seat move from the maximum position. It is because the velocity is zero at the maximum position. When the sinusoidal motion starts, the velocity won't increase rapidly at the beginning. The acceleration spike would be reduced. The maximum position is the ending position. Since

the position of motor is corresponding to the voltage input, the maximum voltage represents maximum positions of translation. As the voltage starts from the maximum, the motion either starts from end 1 or end 2. For instance, it starts from end 1 and move towards end 2, and then it will go back to end 1 to complete a full cycle. Therefore sine waves were created to start at the maximum voltage. A phase shift function was added in the waveform generator VI in the LabVIEW program for generating sine waves. A 90° phase shift was set in. As a result sine waves started generating at the maximum. The experiment verified the jump reduction (Figure 2-7).

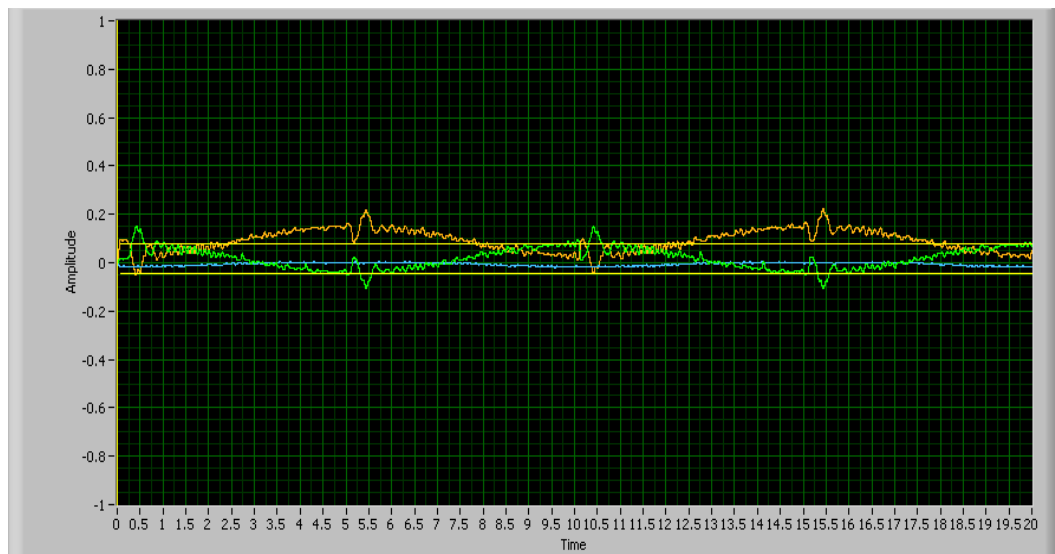


Figure 2-7 a linear acceleration at 0.1Hz with removed overshoot. Green and Yellow sine curves represent the linear translation of test seat measured from two accelerometers respectively. Two acceleration curves were out of phase because their measuring directions were aligned oppositely to each other.

The frontal panel of LabVIEW program in Figure 2-8 shows the sinusoidal signal for the linear translation.

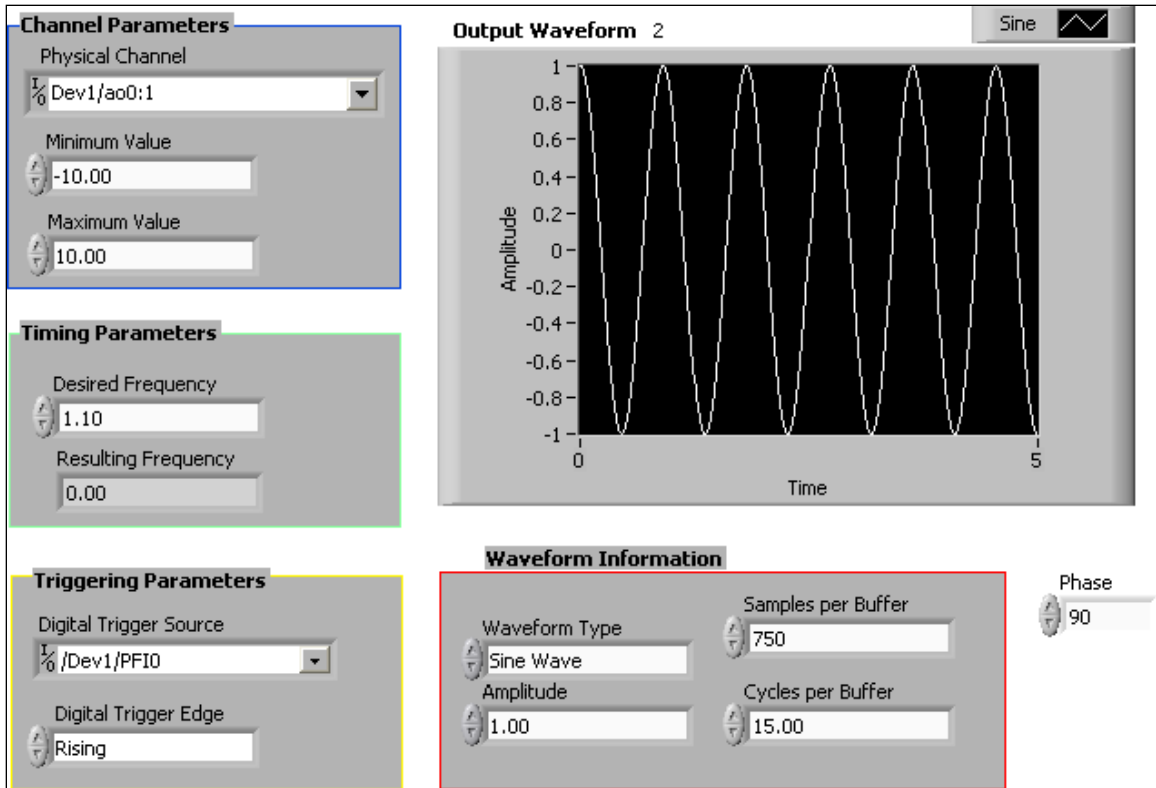


Figure 2-8 Frontal panel of LabVIEW program to generate the sinusoidal signal

Both LabVIEW and PowerTools 5.0 were used to achieve controlling the movement of carriage. As an analog input, the sinusoidal signal was filtered and magnified by MDS before sent to servo motor. By using analog position mode in Power Tools 5.0, the waveform and frequency of analog input decided the motion profile of carriage. On the other hand, the amplitude of movement depended on the amplitude of signal and its corresponding revolution of motor controlled by PowerTools 5.0. To find the relation between the output of movement and the signal and the revolution, we first conducted the experiment to find the amplitude of movement regarding to the amplitude of sinusoidal signal when revolutions (revs.) were 1, 2 and 3. It was found that the amplitude of movement had an almost linear relation to the amplitude of sinusoidal signal and the

number of revolutions respectively. To save the time and due to the limited length of track, the amplitude of movement with respect to the amplitude of signal was deduced at the resolution of 7 (Figure 2-9).

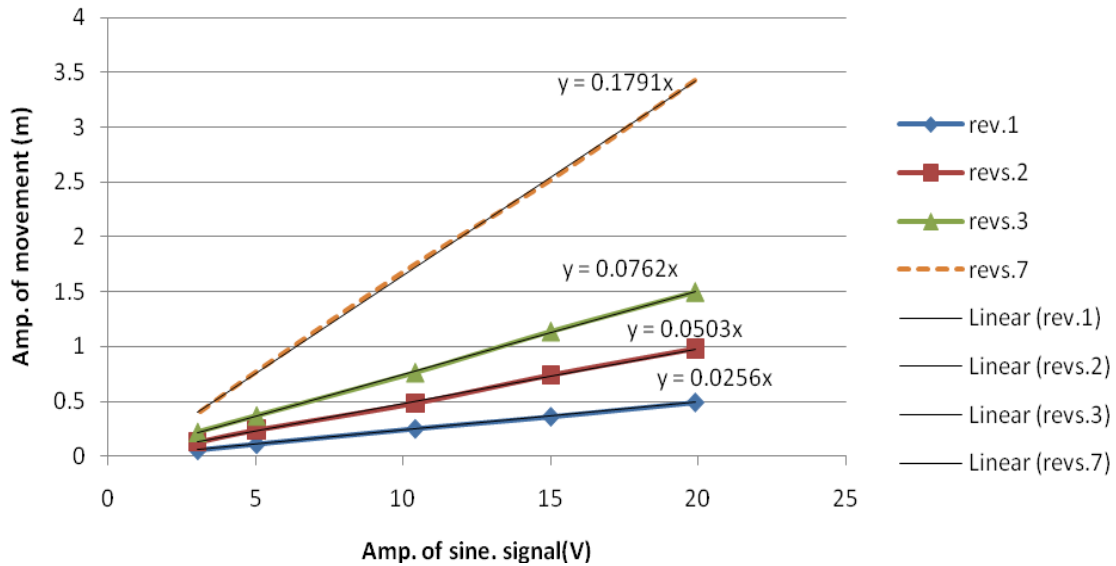


Figure 2-9 configuration of amplitude of carriage movement. Markers represent the amplitude of movement manually measured in the experiment. The dotted orange line represents the amplitude of movement deduced at 7 revs. Overlapping black lines and equations on the basis of linear regression model are predictions of the relation between movement and signal.

2.3 Visual Stimuli

A 3-dimensional visual field was generated during the experiment to portray a recognizable visual scene. A virtual reality head-mounted display (HMD) was designed to display the visual scene of the current test environment simultaneously. This scene was completely controlled by the experimenter. The visual stimuli were different from those used in many previous studies of visuo-vestibular interactions. Earlier studies have tended to either use video recordings provided by HMD, or use patterns of stripes, dot clusters, or geometric figures. Therefore the visual stimulus in this study keeps the higher reality of visual context. The HMD consists of a light-weight helmet, a gimbaled mini

camera and a pair of visual goggles (Figure 2-10). The camera (203CA-1, Pine Computer, CA) was mounted at the top of the helmet through a holder with multi-degree freedom. As a result, the camera is able to provide various directions of live-feed input to the virtual goggles. This helmet also serves as the base for attaching accelerometers and photo targets. The goggle (I-glasses HR920-3D, 920,000 Pixels per LCD, i-O Display Systems, Sacramento, CA) provides subjects the required visual reality (VR) inputs taken from the mini-camera.



Figure 2-10 (a) A helmet with a gimbaled mini-camera mounted on the top. (b) Virtual

2.4 Data Collection and Processing

2.4.1 Accelerometer

Acceleration is measured by accelerometer. To choose a proper accelerometer, several concerns are included. Motion stimuli in the system can be considered as a periodic oscillation with small momentum at a low frequency. The accelerometer needs to sense both acceleration and deceleration, and it must measure low acceleration with good accuracy. Beside, head movement was expected to include both translational and

rotational acceleration. The accelerometer should not just sense the translation, but also has the ability to sense rotation. To protect the natural head movement, accelerometers need to be small and light-weighted. At last, a customer-friendly interface with the accelerometer would help us easily obtain and process the acceleration-related signal.

Three low g types of accelerometers with evaluation board offered by Analog Device were finally applied into the system. They were ADXL320EB, ADXL321EB and EVAL-ADXL335Z. The first two types of accelerometers were used for first two subjects. To obtain higher sensitivity of acceleration, the third type of accelerometer was then introduced into use for last two subjects once it became available. These accelerometers are 20mm×20mm. They have 3 mg resolution at 50Hz and good sensitivity accuracy. Each accelerometer only costs \$30. They are multiple axis accelerometers with signal conditioned voltage outputs.

ADXL320EB measures acceleration with a full-scale range of $\pm 5g$. It was first used to measure the acceleration of seat. ADXL321EB measures acceleration with a full-scale range of $\pm 18g$. It was first used to measure the head acceleration. We initially assumed the head acceleration would have been much higher than that of motion stimuli. The assumption proved to be wrong. The acceleration of the head and seat was more or less same. Both ADXL320EB and ADXL321EB are dual axis accelerometers. EVAL-ADXL335Z is the triaxial accelerometer. It measures the acceleration of $\pm 3g$ at each

direction. All accelerometers have a factory-installed 100nF capacitor at the output of each direction channel to reduce the bandwidth to 50Hz (Figure 2-11).

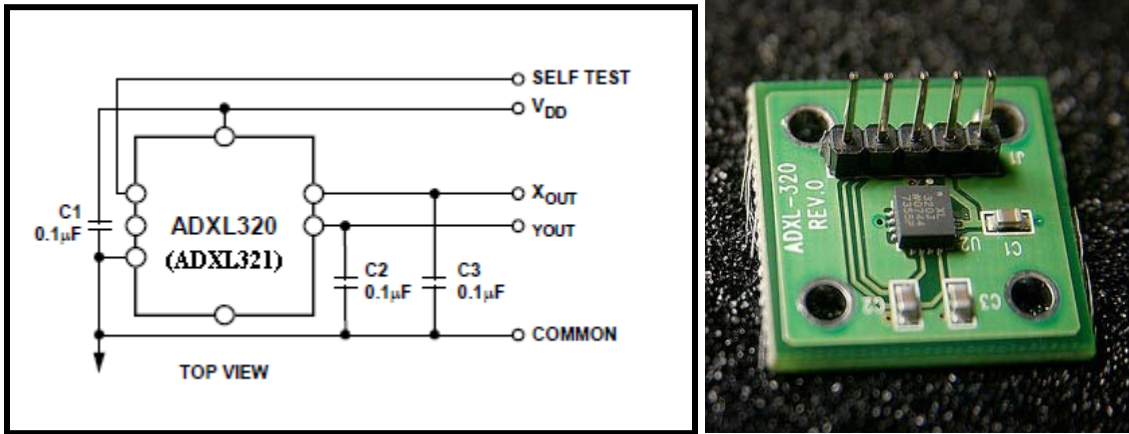


Figure 2-11 ADXL320EB and ADXL321EB. Left is the schematic diagram. Right is the real product.

Each accelerometer needed to be first calibrated before put into use. These accelerometers were applied to the motion with very low frequencies (less than 2 Hz). There are two methods to calibrate low-g accelerometers. The first method can use the shaker to provide the vibration with experimental frequency and use a calibrated and high-profile sensor to provide reference acceleration. However the shaker available in our department cannot provide consistent vibration at the frequency below 10Hz.

As an alternative method, we calibrated them through the use of the industry standard tumble test from IEEE-STD-1293-1998. The tumble test takes gravity as one reliable source of stimulus for calibrating accelerometers with full-scale ranges of less than 20g, based on the need for the calibration stimulus to equal 5% or more of the full-scale range. (Carver and Looney 2007) Given the low-g acceleration was expected in this study, the

basic 4-point tumble test was used for calibration (Figure 2-12). The calibrating direction X was first aligned with the gravity and the X-axis output was recorded. Then the direction was shifted counter-clockwise by 90°, 180° and 270° and X-axis output were respectively recorded.

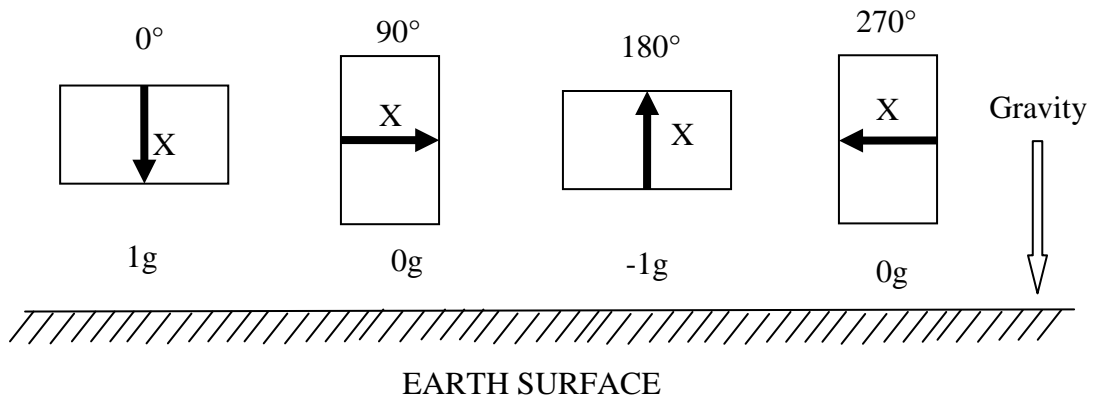


Figure 2-12 Four-point tumble test for X direction

The raw output from an accelerometer is a voltage signal. The calibrating circuit was designed shown in Figure 2-13.

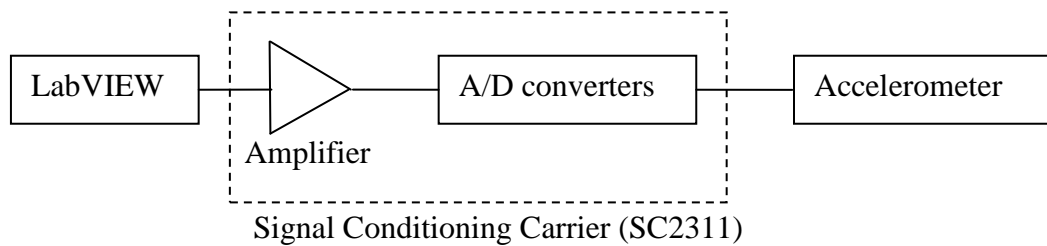


Figure 2-13 acceleration calibrating circuit

The purpose of calibration is to derive a linear relationship between voltage and acceleration as shown in Eq.4.

$$a_g = ma_v + b \quad (4)$$

- a_g : acceleration in the unit of g
- a_v : acceleration in the unit of V
- m : linearity
- b : offset

With recorded measurements of X-axis acceleration at four positions in Figure 2-12, we can find m and b by Eq. 5 and 6.

$$m = \frac{1}{2}[a_g(90^\circ) - a_g(270^\circ)] \quad (5)$$

$$b = \frac{1}{2}[a_g(0^\circ) + a_g(180^\circ)] \quad (6)$$

The value of m and b would serve as conversion factors for the data acquisition system. The conversion factor would be inserted into the data acquisition program. As a result the acceleration value was directly collected by the unit of g. Derived conversion factor of accelerometer varies along with different signal amplification in the signal conditioning carrier. Conversion factors for accelerometers are listed in Appendix B. At last we verified the measurement of calibrated accelerometers by the idea that flipping over the direction of accelerometer over 180 degree would cause a 2g difference in this direction.

2.4.2 Motion tracking system

The motion tracking system includes a high-speed Phantom V4.2 camera (Vision Research) and Phantom[®] 630.A software. The Phantom provides 8-bit image depth and can record up to 2,100 frames per second at a full resolutions of 512×512 pixels. The Phantom V4.2 camera uses a CMOS sensor to remove the blooming effect. The exposure time is variable and independent of sample rate. Capture could be triggered by short-circuiting the 5V trigger cable of camera. The 10/100/Gigabit Ethernet interface provides the communication between the camera and a computer. A 1” zoom lens Doz-10X16

(Navitar) is mounted to the Phantom V4.2. Field of view of these lenses are widely adjustable from 16 to 160mm. The focusing range of lenses is able to change from 1.5m up to ∞ . Phantom[®] 630.A provides the camera control in Windows XP environment. The image capture and recording option under the acquisition pull down menu displays a dialogue window showing exactly what the Phantom camera is capturing in a live preview mode.

The Phantom camera is placed transversely to record the displacement of subject in the longitudinal axis (Figure 2-14). To determine the Lens Focal Length, the following factors must be concerned:

- Focal length (FL): The distance between the camera sensor and the center of the lens. The greater the focal length, the larger the image will appear.
- Field of View (FOV): The size of area to be imaged. In our experiment at least 3m field of view is required to be covered in order to record the whole sinusoidal motion at 0.1Hz.
- Working Distance (WD): Distance from the camera lens to the area under surveillance.
- CMOS: The size of the camera's image sensor device.

A formula is applied to calculate the FL:

$$FL = \frac{CMOS \times WD}{FOV} \quad (7)$$

We have 1" C-mount CMOS camera. The limited space of experimental environment doesn't allow us to change WD in a large scale. Both WD and FL have to be adjusted to

achieve the 3m clear coverage. The displacement of subject during each test is recorded and saved by Phantom software.

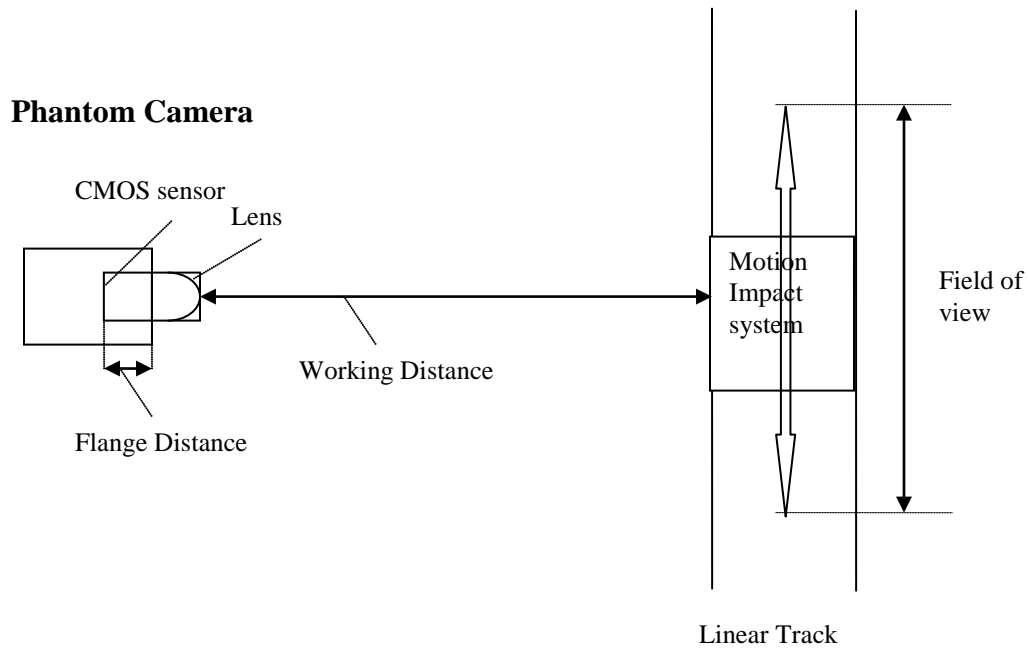


Figure 2-14 Phantom camera layout

2.4.3 Data Processing

The nature of data processing was to quickly obtain the information of interest from raw data. We were interested in the amplitude, phase and offset of acceleration of the head, trunk and seat, as well as the displacement of the head and seat. It would be extremely time-consuming if we manually process acceleration data on a spreadsheet. Therefore a set of Matlab programs were used to process acceleration data. (Appendix C) To remove the noise from motor and environment coupled into the acceleration measurement, and given that the head-neck system could be considered as a second-order system with linear constant coefficients, a linear regression model was used to smooth the acceleration and to predict parameters such as amplitude and phase, offset of the acceleration. To

investigate its frequency components, the predicted acceleration underwent Fast Fourier Transform (FFT). The schematic diagram of processing acceleration data is shown in Figure 2-15. These Matlab programs generated two formats of output: spreadsheets and figures. Predicted acceleration and its frequency response can be saved in Excel file and be illustrated by plotting it.

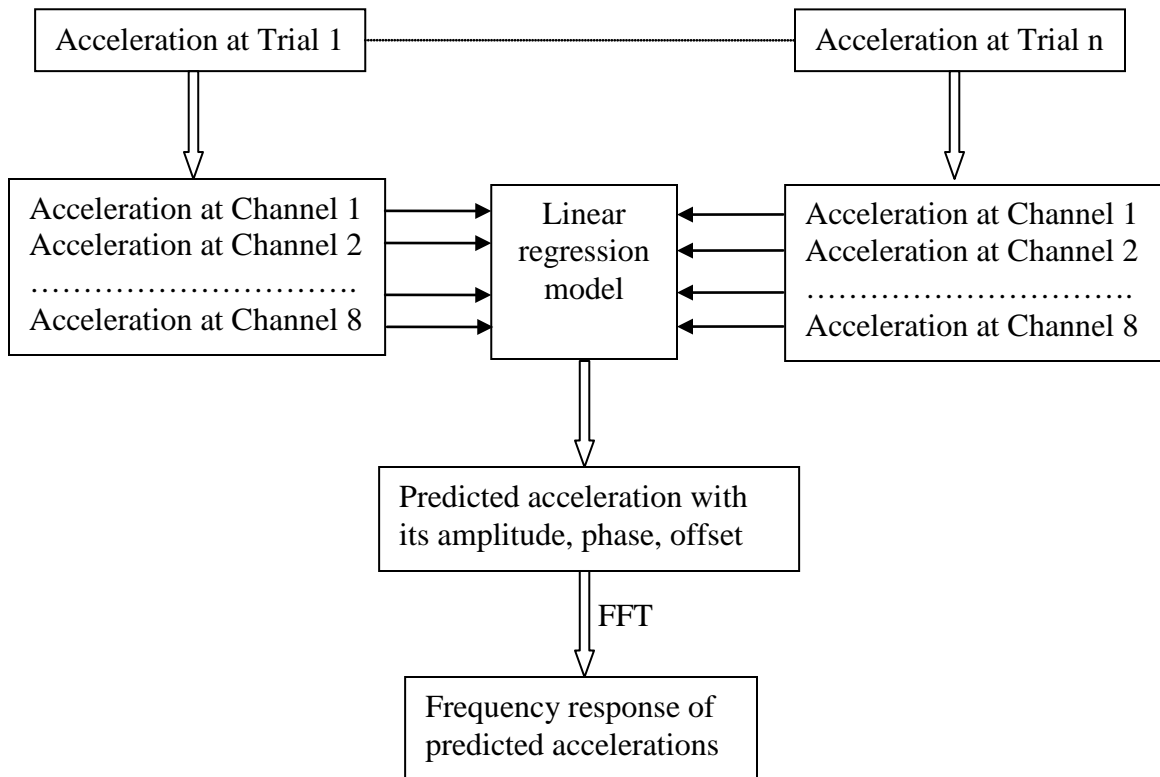


Figure 2-15 the scheme of processing acceleration data

Data processing also achieved the frame transformation. Acceleration of the sled was measured under the world frame. Acceleration of the head was measured under the local frame. There was an initial rotation angle between the world frame and the local frame. Since accelerations under different frame can't be compared. Therefore a transformation matrix was used to transform acceleration of the head from its current frame to the world

frame (Figure 2-16). Acceleration of the head is a vector in space. A transformation law for Cartesian components of vectors was used to transform the vector to the world frame (shown in Eq.8-Eq.10).

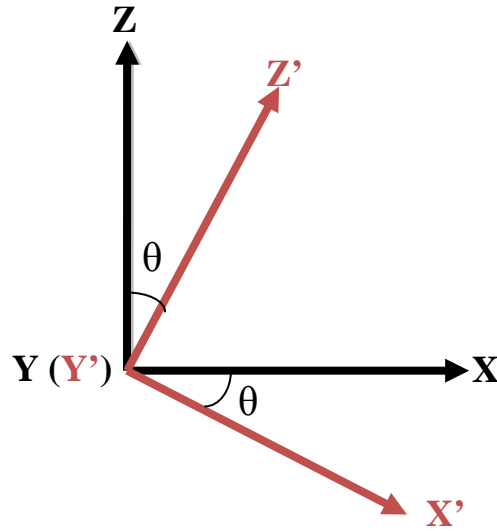


Figure 2-16 right-hand rotation of head about Y axis by an angle θ . Here the unprimed and primed frames represent world and local frame respectively.

$$[a] = [Q][a]' \quad (\text{Lai, 1993}) \quad (8)$$

- $[a]'$ is acceleration of the head under the local frame.
- $[a]$ is acceleration of the head under the world frame.
- $[Q]$ is transformation matrix.

To find $[Q]$, we have

$$\begin{aligned} e_x' &= e_x \cos \theta + e_z \sin \theta \\ e_y' &= e_y \\ e_z' &= -e_x \sin \theta + e_z \cos \theta \end{aligned} \quad (9)$$

Then we get

$$[Q] = \begin{bmatrix} \cos \theta & 0 & -\sin \theta \\ 0 & 1 & 0 \\ \sin \theta & 0 & \cos \theta \end{bmatrix} \quad (10)$$

The displacement of movement was obtained by using image processing technique. Motion of the head and seat were recorded as film clips by Phantom camera. The high-resolution film was converted to images by Phantom software. Vision Assistance 9.0 (National Instruments) was used to calculate the displacement of markers placed on the head and the tip of seat (Figure 2-17). The feature of batch processing in Vision Assistance helped obtain the displacement from thousands of images in a very short time. However, due to limited field of view caused by the space and size of lens, the camera only captured the part of movement at certain frequencies. All data such as the amplitude and phase of acceleration and the displacement were finally put into EXCEL sheets for further investigation.

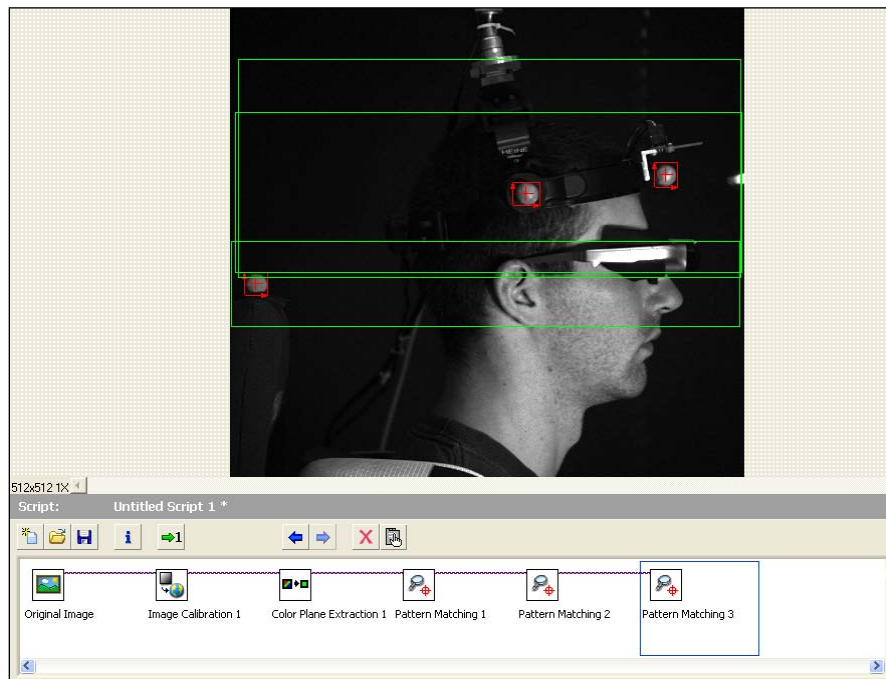


Figure 2-17 Image processing motion of the head and seat.

CHAPTER 3

PILOT STUDY

3.1 Study concerns

The motion of the head neck complex mainly occurs in mid-sagittal plane when the entire body in the sitting posture is exposed to A-P translations. (Fard *et al.* 2003, Paddan and Griffin 1988) The pilot study included four young healthy subjects to examine the effect of combined A-P translation and visual inputs on the head movement. The focus of the study was the relationship between acceleration of the head and trunk. For the first two subjects, two accelerometers (#1 ADXL321EB-1, #3 ADXL321EB-2) on the HMD (one is on the temporal site, another is on the frontal site) measured local head accelerations. A third accelerometer (#2 ADXL320EB) was attached to the cubic frame to measure acceleration of the seat. To improve the validity of measurement and with more selection of accelerometers available as well, biaxial accelerometers placed on the HMD were replaced with two new triaxial accelerometers (#4 EVAL-ADXL335Z-1, #5 EVAL-ADXL335Z-2) for the last two subjects. An accelerometer (#6 ADXL320EB) was attached to the chest and one (#7 ADXL 321EB-2) was attached to the seat. Photo markers were placed to record displacement of the head and seat (Figure 3-1).

To describe the head motion, an anatomical description of direction was used in the design of the experiment and applied to the results. Anterior-posterior (A-P) direction represents X direction, medial-lateral (M-L) direction is Y direction, and up-down (U-D)

is Z direction. The angular acceleration of head-neck system was derived from linear acceleration in related directions.

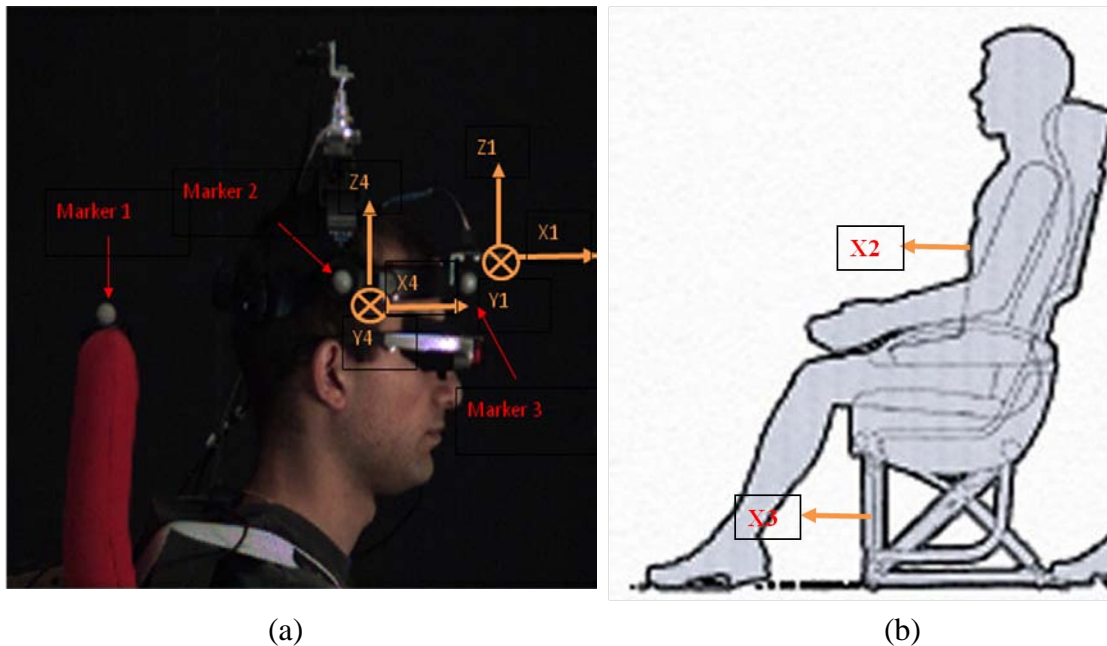


Figure 3-1 Acceleration data collection (a) Accelerometers 1 and 4 on the head. (b) Accelerometer 2 on the torso and an accelerometer 3 on the sled. Cross lines at 1 and 4 mean that their Y directions point inward.

3.1 Subjects

Four young healthy subjects participated in pilot experiments (Table 1). Two subjects were undergraduate students who were unaware of the apparatus' abilities. Two subjects were graduate students. One was aware of apparatus' abilities but not of the current experimental procedure and goals. The other was a laboratory member who was familiar with both apparatus' abilities and the experimental procedure. All subjects have given informed consent approved by the IRB at Temple University before undergoing the experimental protocol. Subjects have a minimum of 20/40 corrected vision in each eye and have no current or history of neurological disorders, and have adequate hearing.

Table 1 Physical characteristics of subjects (the # represents the subject number)

subject	#1	#2	#3	#4	Mean
Age (yr)	26	25	25	22	
Height(m)	181	184	185	183	
Weight (kg)					

3.2 Design of Experiment (DOE)

Motion stimuli in the study were configured with the following four sinusoidal frequencies (0.1, 0.2, 0.5, 1.1 Hz) (Table 2). The magnitude of acceleration at each frequency must meet two requirements. First, it must be large enough to activate the sensitivity of vestibular/proprioceptive receptors reported by literature (Walsh 1960). Second, the magnitude must be tolerated by subjects. We also took into consideration the configuration of motion used in the preliminary study. (Appendix A) The peak velocity and peak acceleration was controlled to characterize the sensitivity of velocity-sensitive visual receptors and acceleration-sensitive vestibular/proprioceptive receptors respectively at different frequencies. Due to the limited length of WH120 and safety concerns, peak acceleration was equalized among 0.2Hz, 0.5Hz and 1.1Hz along with equalized peak velocities at 0.1Hz and 0.2Hz. By controlling the acceleration parameters of the input, we have kept the sensitivity of vestibular/proprioceptive receptors the same so that the effect of visual receptors to head motion can be studied.

Table 2 Configuration of Motion Stimuli

Freq.(Hz)	Angular freq. (w)	Amp. Of sine wave (V)	Revs. of motor	Amp. (m)	Accel. _{max} (g)	Accel. _{max} (m/s ²)	Vel. _{max} (m/s)
0.10	0.63	8.2	7	1.500	0.06	0.59	0.942
0.20	1.26	4.1	7	0.750	0.12	1.18	0.942
0.50	3.14	5	1	0.120	0.12	1.18	0.377
1.10	6.91	0.9	1	0.024	0.12	1.15	0.166

The displacement of sinusoidal motion x :

$$x = A \cos(\omega t), \quad \omega = 2\pi f \quad (11)$$

- f is the frequency of sine wave;

- ω is the angular frequency of sine wave.

- t is the time of test period

- A is the amplitude of sinusoidal motion

The corresponding velocity:

$$v = -A\omega \sin \omega t \quad (12)$$

The corresponding acceleration:

$$a = -A\omega^2 \cos \omega t \quad (13)$$

The purpose of the study was to find the effect of two kinds of treatments (motion and visual stimuli) on pitch acceleration of the head. There were two independent variables: frequency of the sine wave and direction of visual inputs, and one dependent variable pitch acceleration. As shown in Table 3, motion stimuli were a four-level treatment which had four frequencies 0.1Hz, 0.2Hz, 0.5Hz and 1.1Hz, and visual stimuli were also a four-level treatment which has four sets:

- 1) EO -- Eyes open and VR was in phase to A-P translation
- 2) SW -- VR was aligned with M-L direction.
- 3) BW -- VR was 180° out of phase to A-P translation.
- 4) EC -- Eyes closed and VR turned off.

Each level from two treatments was combined to one another. 16 experimental conditions were created. Each condition was repeated twice to validate the measurement. Totally 48 runs were performed to a subject study.

Table 3 Experimental Matrix

Frequency of motion stimuli (Hz)	Visual Conditions			
	EO	SW	BW	EC
0.1				
0.2				
0.5				
1.1				

Experimental Challenges

Ideally experimental runs were to be randomized. This means that the operating frequency of 0.1Hz in this run may either not appear in the previous run or in the next run. However changing the frequency from 0.5Hz or 1.1Hz to 0.2Hz or 0.1Hz needs to adjust not only the resolution of motor from 1 to 7 but also the voltage of sinusoidal signals. It took 20 seconds or more to update the new resolution of motor and any mistake in following the experimental steps may cause the sudden displacement of seat. To save experimenting time and also to ensure the complete safety of experiment, we decided not to use this randomization of conditions. In this study, frequencies of motion stimuli were randomized between and within two groups. The first group was 0.1Hz and 0.2Hz. The second group was 0.5Hz and 1.1Hz. Then four visual inputs were randomly and equally selected for each experimental condition. The arrangement of experimental conditions was displayed in Appendix D.

As a necessary part of experimental design, we also want to keep the initial orientation same among trials for each subject. Different orientation of the head at the beginning would increase the difficulty of data verification. Accelerometer locations on the HMD provide us a reference frame to study initial orientation of the head (Figure 3-2). To equalize the initial orientation, we designed a square board and connected it to an accelerometer. A CXM544 orientation sensor (Figure 3-3) was first used to measure the roll, pitch and azimuth angles of accelerometers by aligning one of its surfaces with the square. The subject was asked to be seated with the five-point harness on. Angles of the head were recorded as initial orientation of the head. Then orientation of the head was measured before every trial to ensure the head remained its initial orientation. Angles within $\pm 5\%$ variance met criteria that initial orientation of the head didn't change.

CXM544 was not able to instantly update orientation angles after two subjects were tested. We believe that some components in CXM544 began to break down. Then another approach was used in achieving equalizing initial orientation of the head. We found the comfortable head position of subject when being seated and fastened on the test chair. The method of projection was applied to record the upper edge of square board on two crossing side-walls by using tape bands. As we know two crossing lines in the space form a plane. Once the first initial orientation of the head is recorded, we could align upper edges of square board with these tape bands to equalize the initial head orientation for each condition .

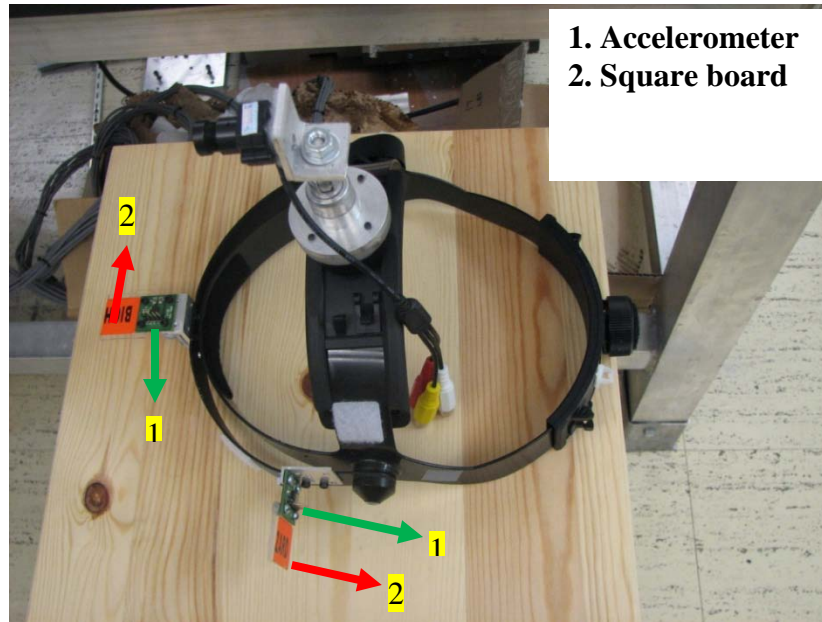


Figure 3-2 Orientation of accelerometers on HMD



Figure 3-3 CXM544 Orientation sensor

CHAPTER 4

RESULTS

Raw acceleration from each channel of accelerometers was processed and plotted in Figure 4-1. In the parameter of prediction, the r^2 coefficient of linear regression model was used to decide how well the acceleration pattern fitted the sine curve. The fitted sine curve is considered representing well the acceleration pattern if r^2 is larger than 0.5. As shown in Figure 4-2, these sine curves which we called predicted acceleration, in most part, represent well the real acceleration. Then based on the predicted acceleration we found the amplitude and phase of linear peak acceleration in all measured directions.

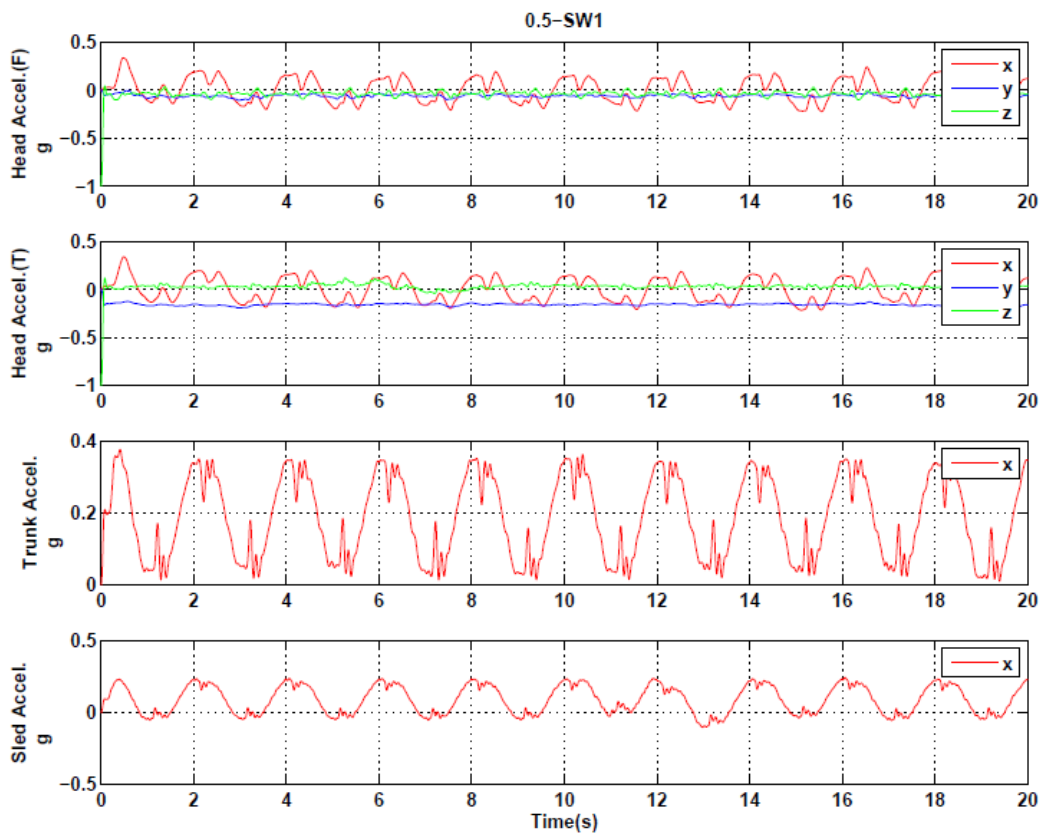


Figure 4-1 Acceleration of the head, trunk and sled with SW at 0.5Hz

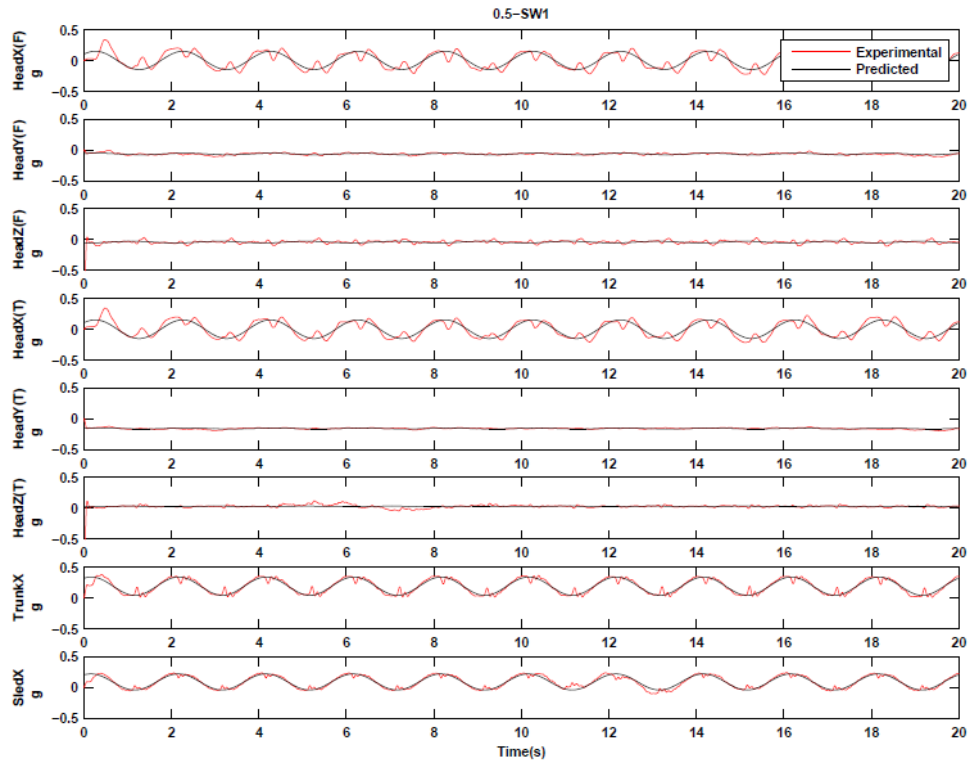
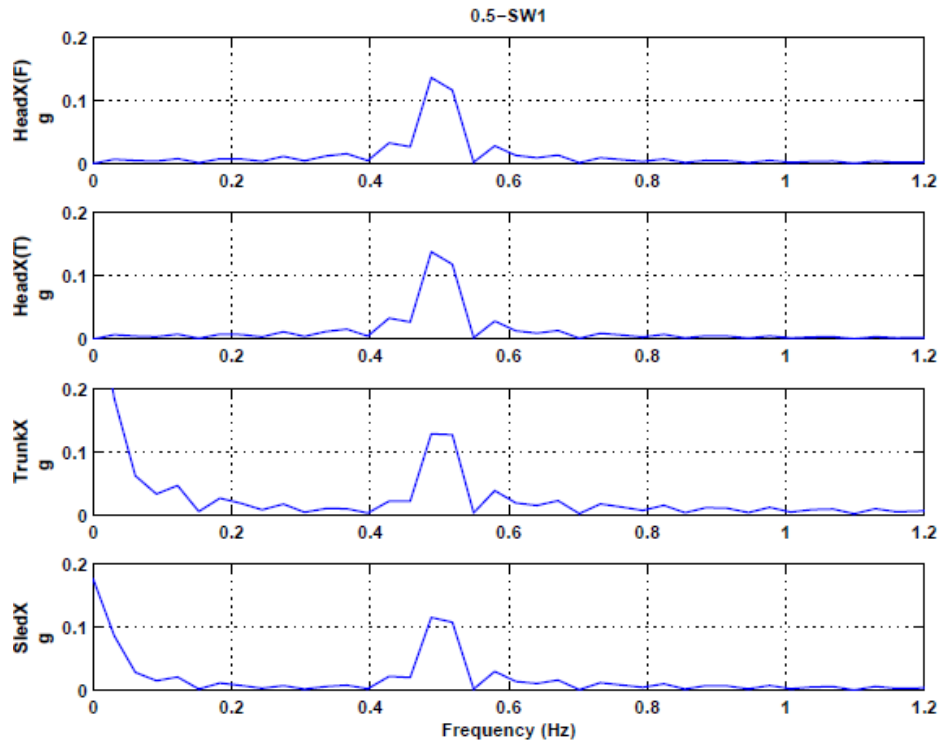
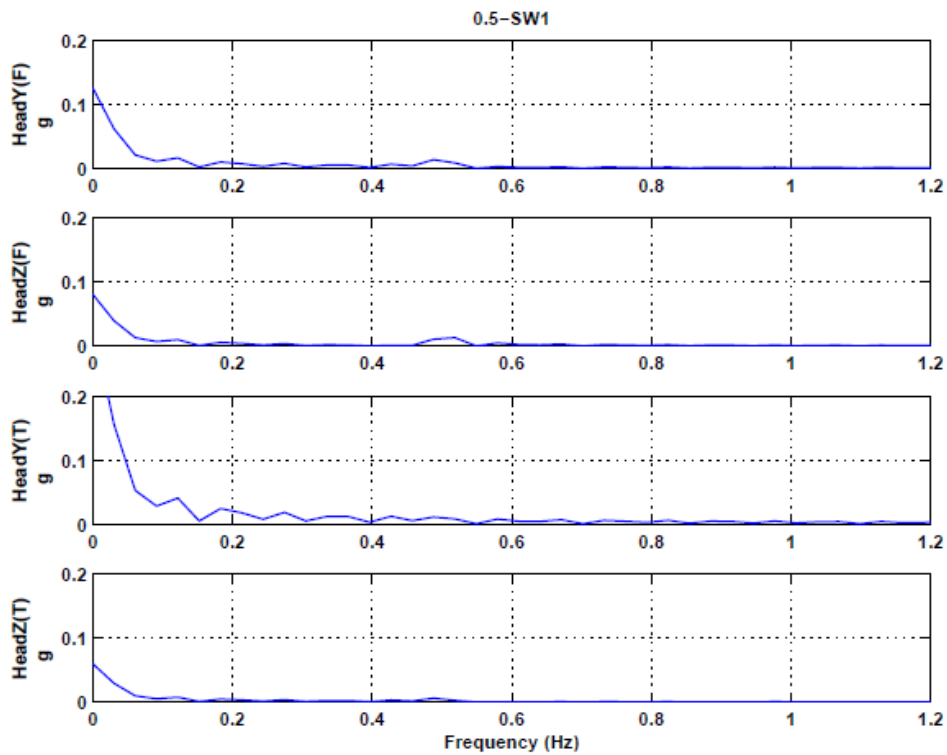


Figure 4-2 acceleration processed by fitted-sine model with SW at 0.5Hz

Fast Fourier Transform (FFT) was applied to find frequency components of head acceleration. The frequency range of motion profile for normal subjects is similar to the range from the preliminary study of patient subjects (Appendix A), where no harmonics of head movement appeared in subjects with motor-neuron disease. Hence we expected to see that there would be no harmonics in the dynamic response of normal subjects. Results justified this expectation. As shown in Figure 4-3, no harmonics appeared in the frequency spectrum of the head in both principal and secondary directions along with all motion profiles and visual conditions. Comparing to the acceleration in the principal X (A-P) direction, the acceleration in the secondary Y (M-L) and Z (U-D) directions was very small.



(a)



(b)

Figure 4-3 Frequency spectrum of acceleration at 0.5Hz and SW (a) Principal direction (b) Secondary direction

Pitch acceleration of the head was also calculated (Eq. 14) since some studies (Gresty 1989, Fard *et al.* 2003) used it to characterize the head acceleration during A-P translation. Frequency response of head pitch acceleration was studied and plotted with acceleration of the sled (Figure 4-4). Gains and phases of head acceleration related to sled were investigated in this study. The trunk was fixed to the sled so acceleration of the trunk is considered equal to that of the sled.

$$a_{pitch} = sign(a_{A-P}) \cdot \sqrt{a_{A-P}^2 + a_{U-D}^2} \quad (14)$$

Comment: As a vector, the direction of a_{pitch} depends on the direction of a_{A-P} which is decided by $sign(a_{A-P})$.

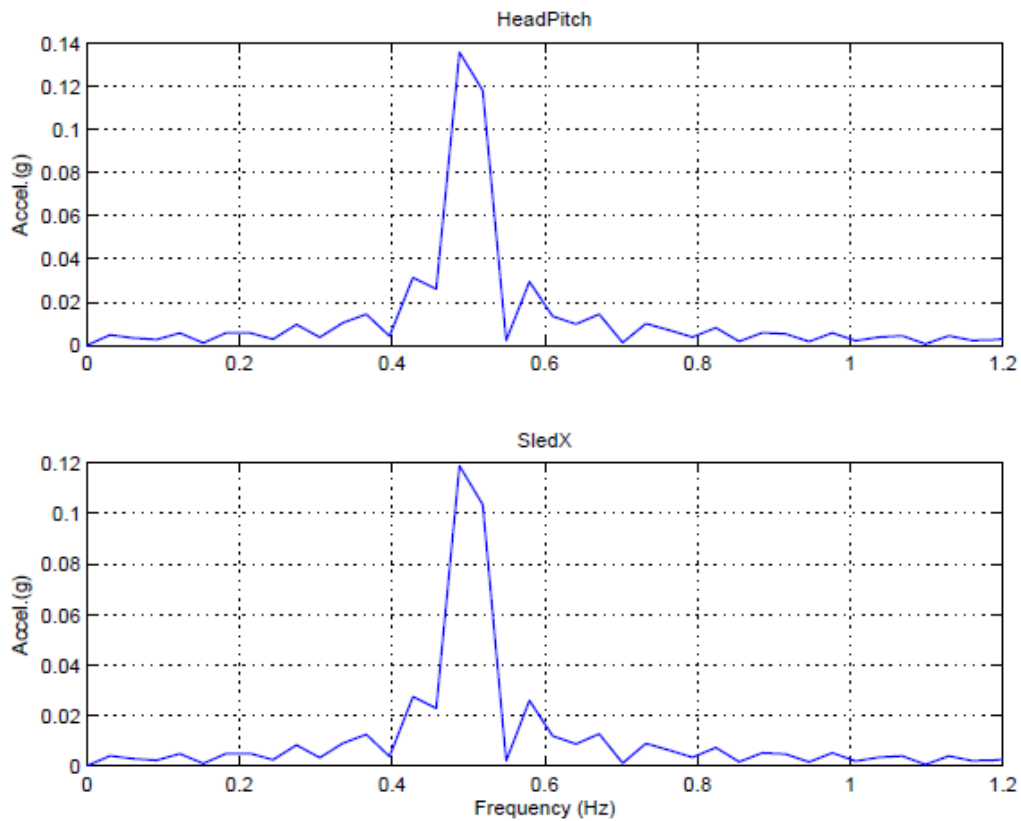


Figure 4-4 head pitch accelerations and corresponding acceleration of the sled and trunk with SW at 0.5Hz.

The non-parametric statistical test was first used in analyzing the effect of frequencies and visual conditions on gains. The non-parametric technique can avoid assuming normal distribution or homogeneity of variance in the subjects involved. With four samples drawn from the same population, the Friedman two-way analysis of variance (ANOVA) by ranks was used to first test the significance of difference of gains among all experimental conditions. *Null Hypothesis* H_0 is that the different conditions in experiment have no differential effect where as *Alternative Hypothesis* H_1 is that the different conditions in experiment have differential effect. The established *Significance level* is $\alpha = 0.05$. The *Sampling distribution* χ_r^2 is distributed approximately as chi square.

$$\chi_r^2 = \frac{12}{N \cdot k \cdot (k + 1)} \sum_{j=1}^k (R_j)^2 - 3N \cdot (k + 1) \quad (\text{Siegel, 1956}) \quad (15)$$

N = number of subjects

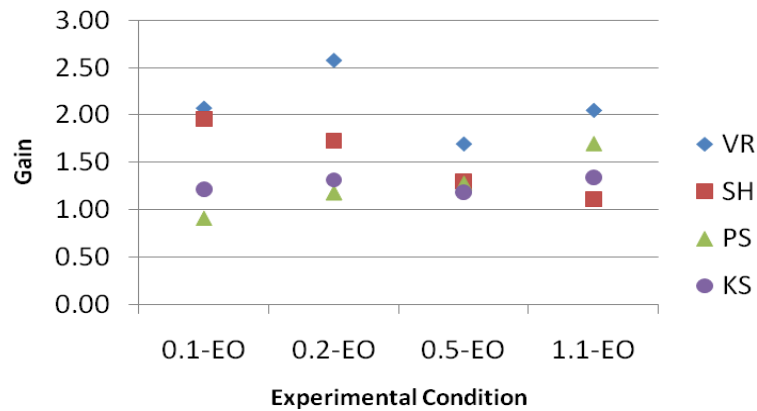
k = number of conditions

R_j = sum of ranks with j th condition

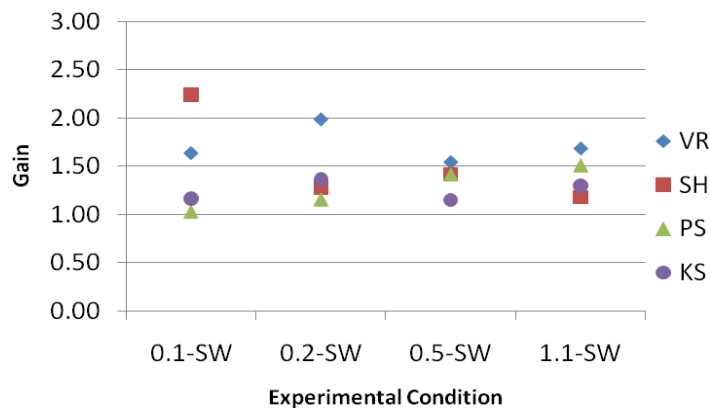
$\sum_{j=1}^k$ directs one to sum the square of the sums of ranks over all k conditions

With $N = 4$ and $k = 16$, $\chi_r^2 = 12.19$. Reference to Table C (Siegel 1956) indicates that the result of χ_r^2 is significant at between the 0.7 and the 0.5 levels of p -value. The $p \geq 0.5$ is larger than $\alpha = 0.05$. Therefore the decision at this level is to accept H_0 . To increase the analysis power, gains were averaged among visual conditions at each frequency. The same Friedman test was used to evaluate the significance across frequencies. In this case, *Null Hypothesis* H_0 is that the different frequencies have no differential effect where as *Alternative Hypothesis* H_1 is that the different frequencies have differential effect. The

level of significance is chosen at $\alpha = 0.05$. With $N = 4$ and $k = 4$, $\chi_r^2 = 3.0$. Reference to Table N (Sigel 1956) indicates that the result of χ_r^2 is significant at $p = 0.432$. The p value is larger than $\alpha = 0.05$. Therefore the decision is to accept H_0 . Overall, no significant difference of gains is believed to be existed among visual conditions across frequencies. However, plots of gains across frequencies in each visual condition (Figure 4.5) show that subjects VR and SH have more scattered gains, and subjects PS and KS have gains close to 1. It may suggest that head of subjects VR and SH is less restricted than that of subjects PS and KS.



(a)



(b)

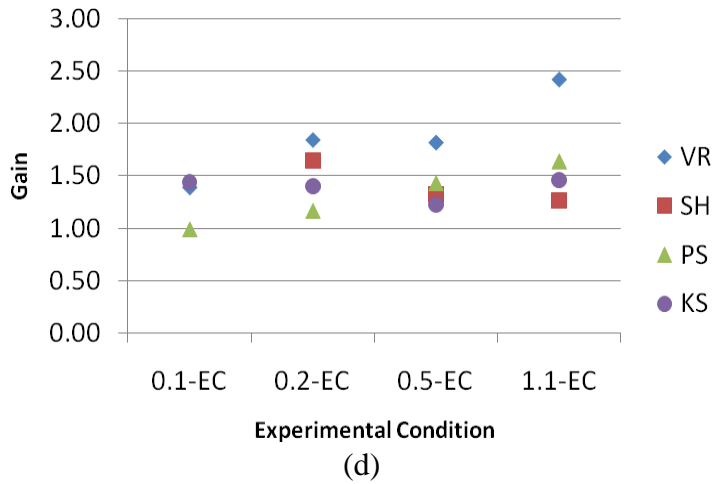
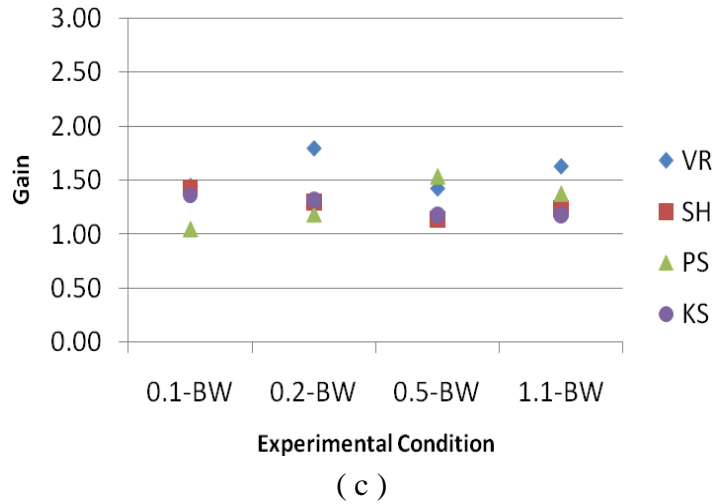


Figure 4-5 gains of head across frequencies in each visual condition. Visual conditions included here: (a) EO (b) SW (c) BW (d) EC

Phase analysis converted the phase of head acceleration relative to sled within the range from 0° to 360° in all experimental conditions. In results shown in Figure 4-6, phases from two subjects VR and SH respond between 90° and 180° and two subjects PS and KS respond the phase close to 0° . Along with suggestion from gain plots, phase results indicate two head strategies were employed by seated subjects. The head of first two subjects was almost locked to sled, and the head of last two was set loose and counter to

motion of sled. This agrees with the report by Vibert et al. (2001) that head-locked or “stiff” subjects show little translation of the head relative to the sled for the whole duration of motion stimuli when the trunk is fixed whereas loose or “floppy” subjects showed a large pitch of the head relative to the sled in the direction opposite to the sled movement. Besides, all subjects show the drop-off phase in the highest frequency.

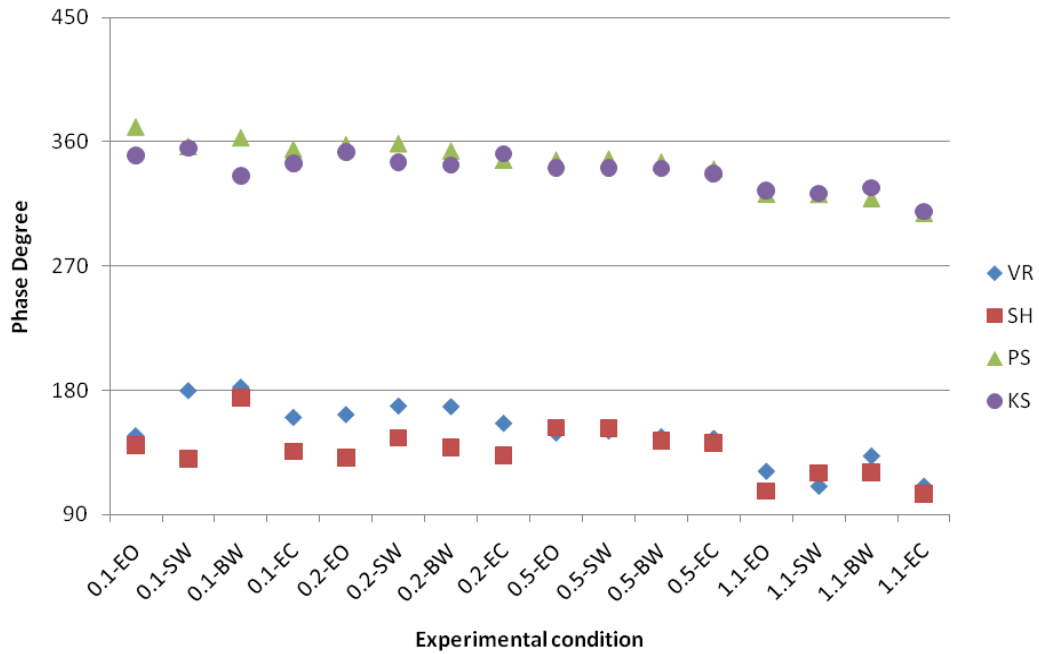
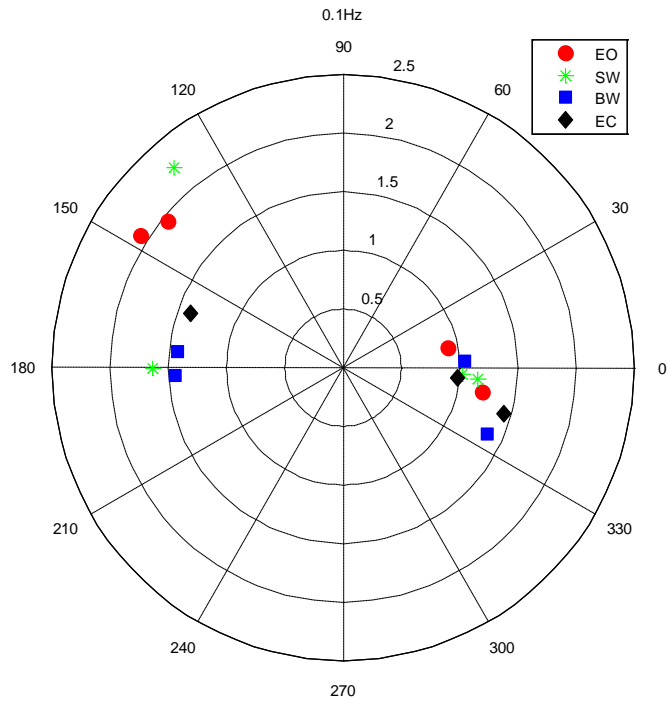
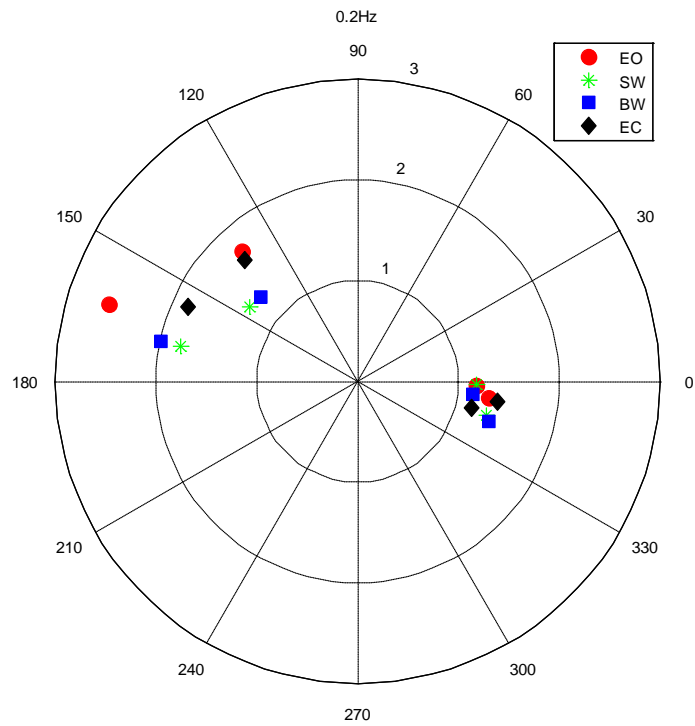


Figure 4-6 phase of head acceleration relative to sled

Polar plots are also used to illustrate two head strategies and more scattered gains in two subjects. First markers on plots from figure 4-7 and figure 4-8 indicate subjects VR and SH have more scattered gains among visual conditions at each frequency. Second markers show there are apparently two head strategies. Subjects VR and SH have the floppy head whereas subjects PS and KS are head locked.



(a)



(b)

Figure 4-7 polar plots of gain and phase of head motion (a) at 0.1Hz (b) 0.2Hz

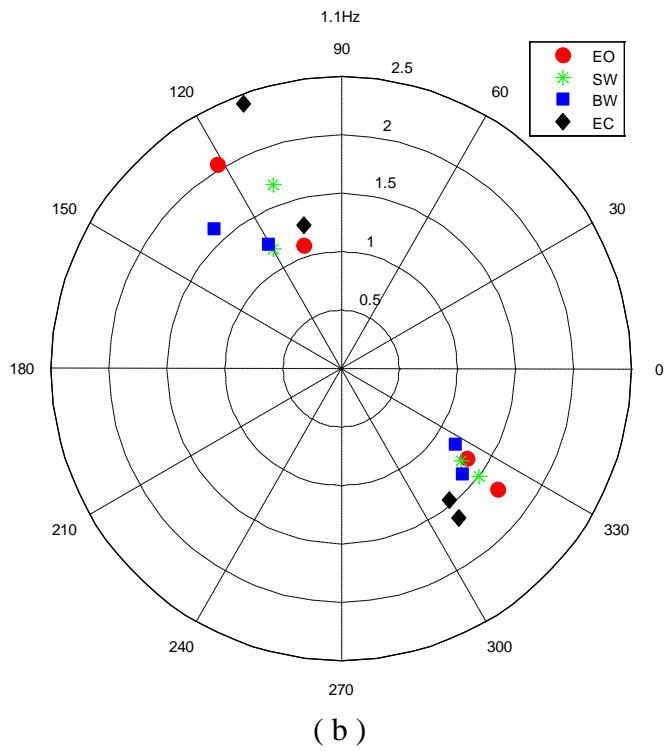
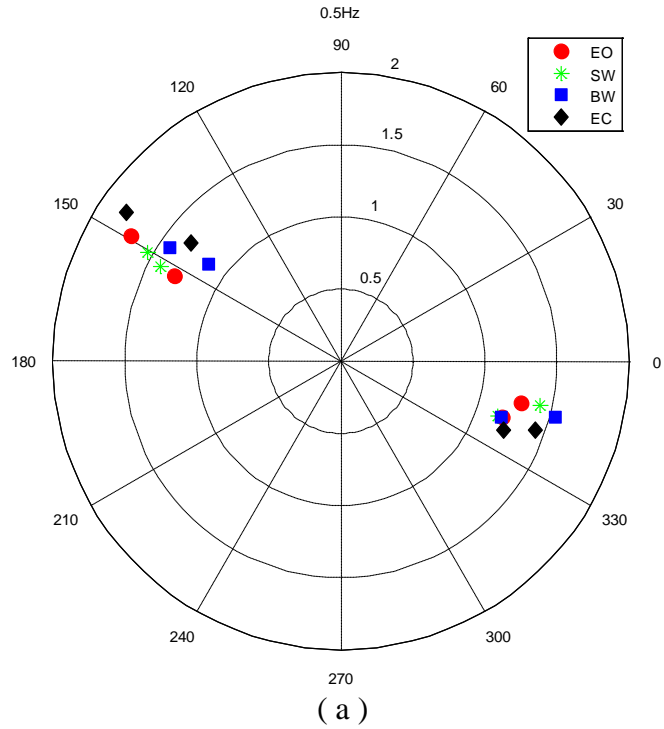


Figure 4-8 polar plots of gain and phase of head motion (a) at 0.5Hz (b) 1.1Hz

To gain more statistical power, a parametric statistical test was also used. 4×4 two-way ANOVA with replication analyzed the effect of frequencies of motion profiles and visual conditions on gains. The averaged gain of head pitch acceleration was plotted against frequency and visual conditions respectively (Figure 4-9 and 4-10). According to ANOVA results (Table 4), the *p*-value of frequency and visual conditions are 0.709 and 0.3556 respectively. Both of them are larger than the significance level of 0.05. Moreover, the *p*-value of interaction between these two factors is 0.987, much larger than the significance level. Therefore there was no statistically significant difference of gain of head pitch acceleration among visual conditions and across the frequency. There was also no interaction between visual conditions and frequencies.

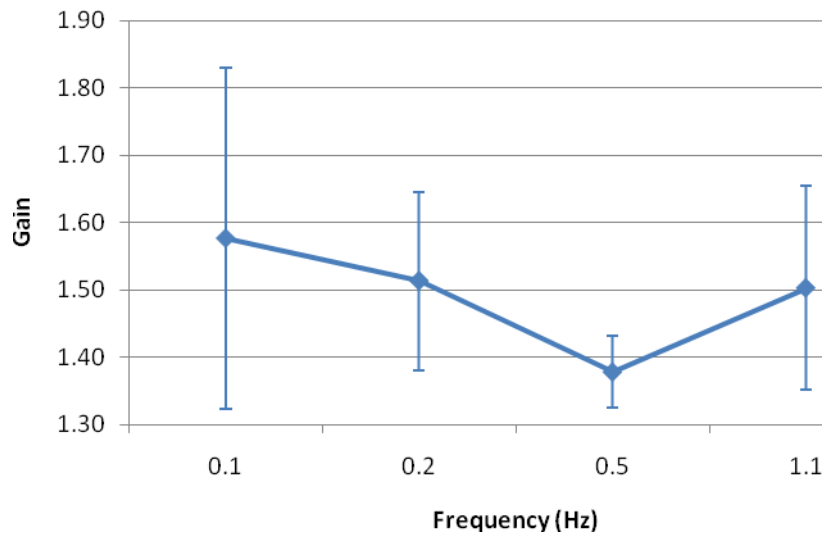


Figure 4-9 Average gain of head pitch acceleration (and standard deviation) with respect to motion frequencies

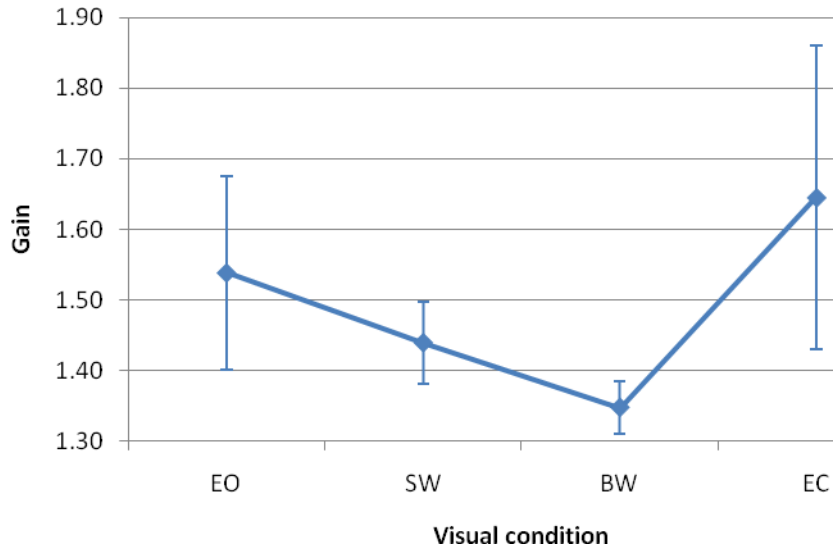


Figure 4-10 Averaged gain of head pitch acceleration (and standard deviation) with respect to visual condition

Table 4 Significance of frequencies and visual conditions and the interaction between them

ANOVA						
Source of Variation	SS	df	MS	F	P-value	F crit
Frequency	0.330606	3	0.110202	0.463285	0.709236	2.798061
Visual	0.789752	3	0.263251	1.106695	0.355618	2.798061
Interaction	0.504749	9	0.056083	0.235771	0.987399	2.08173
Within	11.41782	48	0.237871			
Total	13.04292	63				

CHAPTER 5

DISCUSSION

This experimental system was evaluated through the pilot study. The subjects were tolerant of the motion stimuli. There was no side-effect after they were exposed to the level of stimuli. However there are currently four technical constraints in this system. First, the complete randomization test is not recommended to be conducted. Because it will involve the change of both voltage inputs and revolutions of motor which is time consuming and safety risky. Second, due to the limited length of linear track, the system is unable to equalize the peak acceleration of sled across all frequency points. Third, the linear track was essentially driven by analog signal converted from digital signal programmed by LabVIEW. To achieve the movement at certain amplitude, the signal amplitude has to be pre-set at the desired level in order for programmable motor to execute the expected amplitude. This process is complicate, during which the operator has to be very alert. Any mistake in presetting may cause a sudden jump of sled and the subject might be exposed to sudden shock. Fourth, the selection of subjects was not based on the naivety and diversity of subjects. As a result, any statistical analysis could not assume subjects come from normally distributed population. These issues have to be treated before this study comes to the next stage. As for the experimental protocol, it has been reported that human can be easily adjusted to the sinusoidal motion (Gresty 1989). In future, we would like to include other motion stimuli such as ramp motion, or sum-of-sines (SSN) that consists of relatively prime harmonics of a common base frequency (Keshner 2003).

Self-motion can be induced by using dynamic visual input in the absence of concordant inertial motion. Self motion can be induced even if visual-inertial conflict is present such as during sinusoidal translation (Wright and Schneider 2009). We created the conflict at frequencies equal or less than 1.1Hz. Four visual inputs were applied to subjects, two of which were discordant with inertial motion (SW and BW), one was concordant (EO) and one had no conflict because there was no visual input (EC). Although reports of perceived self-motion were not collected on all subjects, at least one subject remarked that he perceived diagonal side-to-side self-motion during the sideways visual condition. However, statistical analysis on the gain of head acceleration indicated that the conflict didn't have a significant effect. The finding indicates that the head kinematics would not be influenced by the motion of the visual field, but since there is a large body of literature that shows that visual input affects postural and motor control, we suspect that the limited field-of-view (FOV) of the HMD may have had reduced the effects of visual inputs. To enrich visual inputs, the following study of head motion recruits a programmable 3D virtual reality. It has a larger FOV HMD to test the role of visual input to head movement.

The pilot studies were conducted to explore the head acceleration response of healthy subjects during A-P sinusoidal translation. The configuration of physical translation was based on a preliminary study investigating the head acceleration response of patient subjects during A-P sinusoidal translation (See Appendix A). The phase-of-head plot (Figure A-4) suggests that patient subjects used the strategy of head locking to control the

head movement during the experiment. However normal subjects used both head-locking and floppy head strategies in the pilot study. Pitch acceleration of the head is mainly attributed to the linear acceleration in the primary A-P direction in normal subjects. However the pitch acceleration is equally weighted in the primary A-P and the secondary U-D directions in patient subjects.

To further study the dynamic response of the head, we can consider the head-neck complex as a mechanical system under forced vibration. The input here was acceleration of the sled in A-P direction and the output here was acceleration of the head in pitch plane. Results show that head had a sinusoidal acceleration when acceleration of the sled was sinusoidal. This suggests that the head-neck complex is in fact a second-order system with linear constant coefficient. This suggestion fits with two models derived from head studies of human (Gresty 1989) and anesthetized cat (Goldberg and Peterson 1986). Both model address factors such as inertia of the head, elasticity and viscosity of the neck muscles in controlling the head movement. However, two responses strategies indicate that there may be more than one control mechanism influencing stabilization of the head which can include voluntary processes (Keshner and Peterson 1995; Paddan and Griffin 1998).

CHAPTER 6

CONCLUSION

Design and usability of an experimental system was demonstrated for study of head motion under integration of visual and physical stimuli. Visual stimuli include (1) eyes open and VR was in phase to A-P translation (EO); (2) VR was aligned with M-L direction (SW); (3) VR was 180° out of phase to A-P translation (BW); (4) eyes closed and VR turned off (EC). Physical stimuli were simple sinusoidal translation configured respectively at 0.1Hz, 0.2Hz, 0.5Hz and 1.1Hz. The pilot study was conducted with four healthy subjects from the same population. Pitch acceleration at the frontal side of head was used to characterize dynamic response of the head. Results show that the gain of head acceleration relative to the seat was close to one with no significant difference among visual conditions across frequencies, and the phase depends on the head strategy each subject used. In this study, two subjects with head-locked strategy had the phase response around 0° whereas two subjects with floppy head strategy responded between 90° and 180°. These differences suggest more than one control mechanism for head stabilization.

REFERENCES

- Alexander, B. H., Rivara, F. P., & Wolf, M. E. (1992). The cost and frequency of hospitalization for fall-related injuries in older adults. *Am J Public Health, 82*(7), 1020-1023.
- Carver, R., & Looney, M. (2007,). MEMS accelerometer calibration optimizes accuracy for industrial applications. Message posted to <http://www.industrialcontroldesignline.com/202602348?printableArticle=true>
- Clément, G. (2005). *Fundamentals of space medicine* Springer.
- Darvish, K., Keshner, E. A., & Wright, W. G. (2008). *Development of a laboratory to explore multimodal control of orientation in space*
- Darvish, K., Shafieian, M., Romanov, V., Rotella, V., Salvatore, J., Michael D., & Blebea, J. (2009). Development of an in vitro porcine aorta model to study the stability of stent grafts in motor vehicle accidents. *Journal of Biomechanical Engineering, 131*(4), 044505-4.
- Fard, M. A., Ishihara, T., & Inooka, H. (2003). Transmission of the translational trunk vibration to the head-neck complex. *JSME International Journal, 46*(1), 116-122.
- Goldberg, J., & Peterson, B. W. (1986). Reflex and mechanical contributions to head stabilization in alert cats. *Journal of Neurophysiology, 56*(3), 857-875.

- Keshner, E. A., & Peterson, B. W. (1995). Mechanisms controlling human head stabilization. I. head-neck dynamics during random rotations in the horizontal plane. *Journal of Neurophysiology*, 73(6), 2293-2301.
- Keshner, E. A. (2003). Head-trunk coordination during linear anterior-posterior translations. *Journal of Neurophysiology*, 89(4), 1891-1901.
- Lai, W. M., Rubin, D., & Krempl, E. (Eds.). (1993). *Introduction to continuum mechanics* (3rd ed.) Elsevier.
- Menz, H. B., Lord, S. R., & Fitzpatrick, R. C. (2003). Acceleration patterns of the head and pelvis when walking on level and irregular surfaces [Abstract]. *Gait & Posture*, 18(1) 35-46.
- Paddan, G. S., & Griffin, M. J. (1998). A review of the transmission of translational seat vibration to the head. *Journal of Sound and Vibration*, 215(4), 863-882.
- Siegel, S. (Ed.). (1956). *Nonparametric statistics* McGRAW-HILL BOOK COMPANY.
- Stevens, J. A., Corso, P. S., Finkelstein, E. A., & Miller, T. R. (2006). The costs of fatal and nonfatal falls among older adults. *Injury Prevention*, (12), 290-295.
- Vibert, N., MacDougall, H. G., Waele, C. D., Gilchrist, D. P. D., Burgess, A. M., Sidis, A., et al. (2001). Variability in the control of head movements in seated humans: A link with whiplash injuries? *Journal of Physiology*, (532.3), 851-868.

WALSH, E. G. (1961). Role of the vestibular apparatus in the perception of motion on a parallel swing. *Journal of Physiology*, 155, 506-513.

Wright, W., & Glasauer, S. (2006). Subjective somatosensory vertical during dynamic tilt is dependent on task, inertial condition, and multisensory concordance. *Experimental Brain Research*, 172(3), 310-321.

Wright, W. G., & Schneider, E. (2009). *Manual motor control during “virtual” self-motion: Implications for VR rehabilitation*

APPENDIX A

HEAD COORDINATION WITH MOTOR-NEURON DISEASES DURING A-P TRANSLATION

This study aimed at understanding how the head movement in a seated occupant with simple harmonic acceleration inputs would change in terms of frequency, visual feedback (eyes open and eyes closed), and two motor neuron diseases (cerebellar disease and bilateral vestibular deficit). We obtained the acceleration data and related data processing Matlab codes from Dr.Keshner's Virtual Environment and Postural Orientation Laboratory. Seven subjects: four with cerebellar disease (CD) and three with bilateral vestibular deficit (BVD) were chosen in this study. Three accelerometers were used in the test, each of which was attached to head, chest and sled respectively. The trunk of subject was constrained to the sled by belts. Three Frequencies were combined with two visual conditions (eyes open and eyes close) to formulate experimental conditions. Three trials were conducted in each condition. Subjects received 180s linear translation in each trial. The configuration of sled acceleration is listed in Table 4.

Table 5 Configuration of Sled Acceleration

Freq.(Hz)	ω	Amp.(m)	Vel.(max) (m/s)	Accel.(max) (g)	Accel.(max) (m/s^2)
0.60	3.77	0.03	0.10	0.04	0.38
0.81	5.09	0.02	0.11	0.06	0.55
1.11	6.97	0.02	0.10	0.07	0.73

Matlab codes were modified to achieve three technical goals. First goal was the frame transformation. Acceleration of the trunk and sled was measured under the world frame. Acceleration of the head was measured under the local frame. The Matlab code plotted

the modified acceleration of head along with acceleration of the trunk and sled. Figure A-1 is an example of the plot of these accelerations.

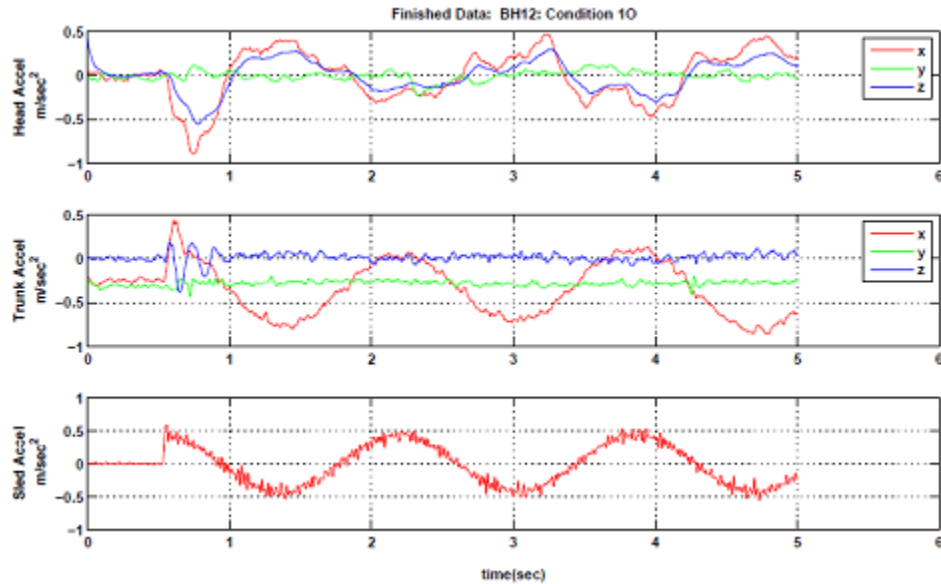
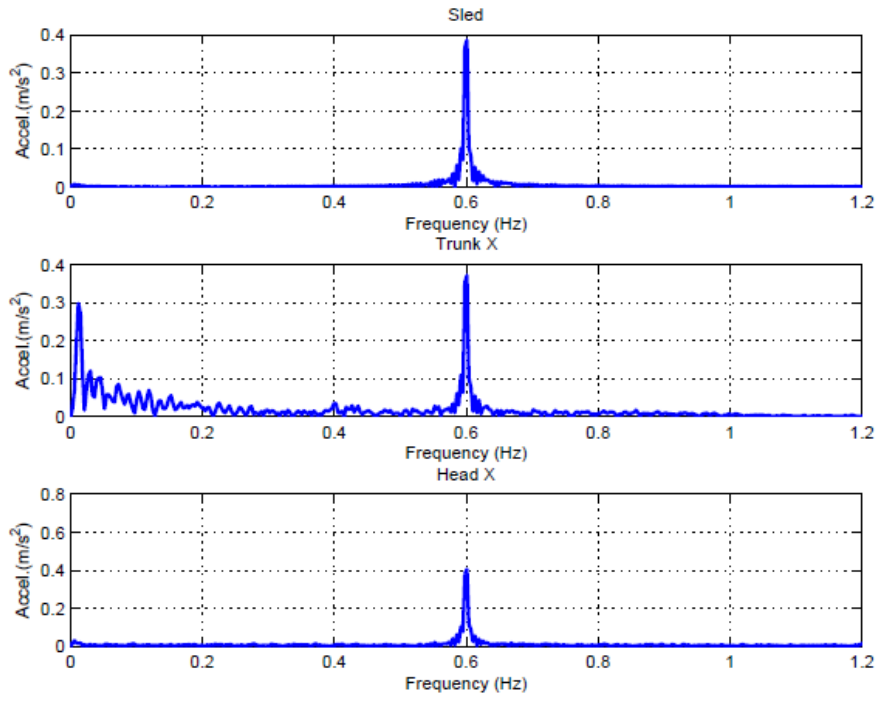
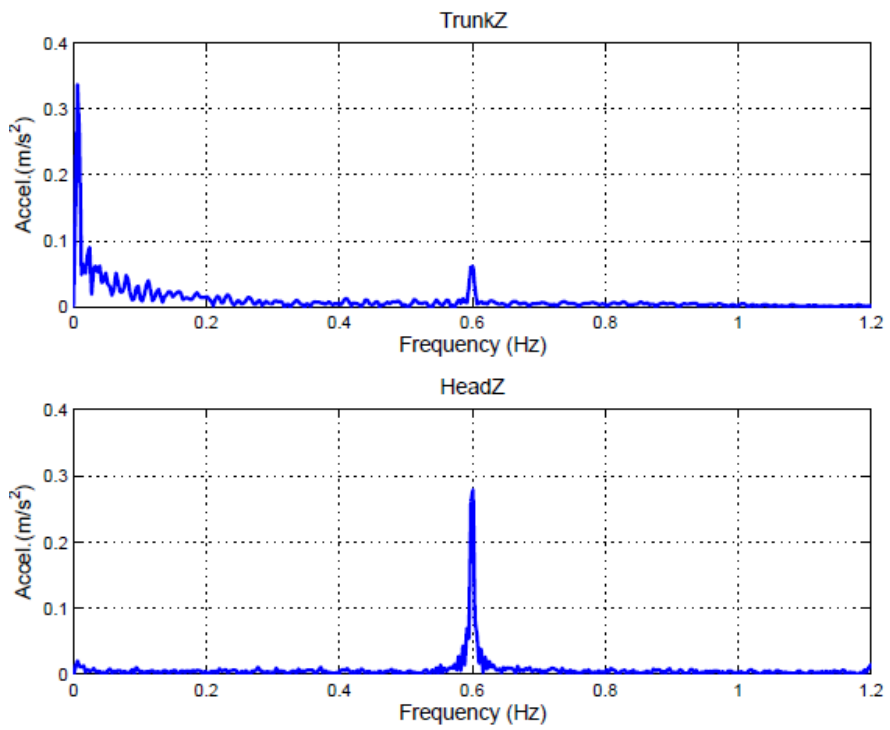


Figure A-1 acceleration of the head, trunk and sled during the first-trial linear

Second, Fast Fourier Transform (FFT) was introduced to find if any mechanical resonance happened to the head during the translation. No harmonics appeared in all three motion profiles and along with two visual conditions. Figure A-2 shows the frequency spectrum of subject DJ at 0.6Hz. However, both Figure A-1 and Figure A-2(b) also show that A-P sled motion caused an oscillatory acceleration of the head in its secondary Z direction. The frequency of secondary acceleration is the same as that of principle A-P acceleration. Two directions also have very close magnitude of acceleration.



(a)



(b)

Figure A-2 frequency spectrum of acceleration at 0.6Hz when eyes were close(a) in the principle direction (b) in the secondary direction

To characterize the head acceleration, pitch acceleration of the head was also calculated. Gains and phases of head acceleration related to sled were investigated in this study. The trunk was fixed to the sled so acceleration of the trunk is considered equal to that of the sled. The non-parametric statistical test was used in analyzing the effect of the frequency of motion stimuli, visual conditions and type of the disease on gains. There are three dependent factors in this study: visual inputs, frequency of physical stimuli and category of disease.

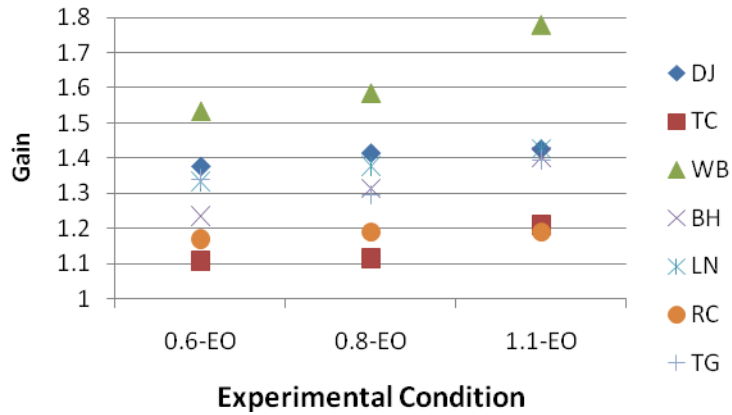
With 7 samples drawn from the same population, the Friedman two-way analysis of variance (ANOVA) by ranks was used to first test the significance of difference of gains among all experimental conditions. Null Hypothesis H_0 is that the different conditions in experiment have no differential effect where as Alternative Hypothesis H_1 is that the different conditions in experiment have differential effect. With $N = 7$ and $k = 6$, $\chi_r^2 = 16.55$. The result of χ_r^2 is significant at between the 0.01 and the 0.001 levels of p -value. The $p \leq 0.01$ is less than $\alpha = 0.05$. Therefore the decision at this level is to reject H_0 and accept H_1 .

To increase the analysis power, gains were averaged among visual conditions at each frequency. The same Friedman test was used to evaluate the significance across frequencies. In this case, *Null Hypothesis* H_0 is that the different frequencies have no differential effect where as *Alternative Hypothesis* H_1 is that the different frequencies have differential effect. The level of significance is chosen at $\alpha = 0.05$. With $N = 7$ and k

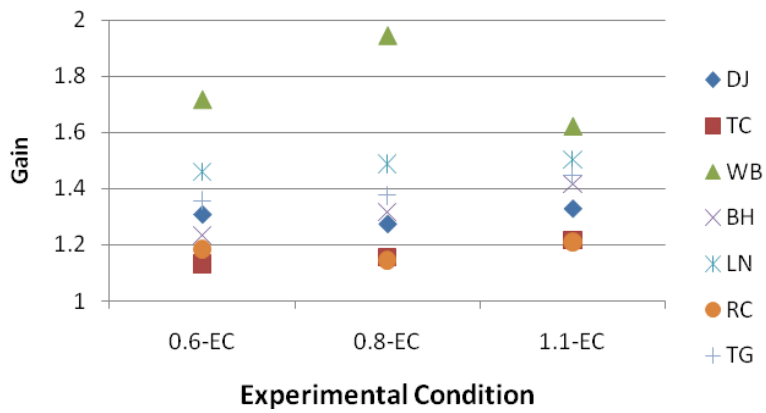
= 3, $\chi_r^2 = 8.857$. The result of χ_r^2 is significant at $p = 0.0084$. The p value is less than $\alpha = 0.05$. Therefore the decision is to accept H_1 . At the first step, a significant difference of gains is believed to be existed among visual conditions across frequencies.

Then to further locate the difference, the Friedman ANOVA was used to test the significance of difference of gains from two groups. The first group included experimental conditions among visual conditions from 0.6Hz to 0.8Hz. . Null Hypothesis H_0 is that the different conditions in experiment have no differential effect where as Alternative Hypothesis H_1 is that the different conditions in experiment have differential effect. With $N = 7$ and $k = 4$, the result of first group χ_r^2 is 4.371. The result of χ_r^2 is significant at between the 0.3 and the 0.2 levels of p -value. The p value is larger than $\alpha = 0.05$. Therefore the decision is to accept H_0 for the first group. The second group included experimental conditions at 1.1Hz. With $N = 7$ and $k = 2$, the result of second group χ_r^2 is 1.286. The result is significant at between the 0.3 and the 0.2 levels of p -value. The p value is larger than $\alpha = 0.05$. Therefore the decision is to accept H_0 for the second group.

Above all the significant difference of gains is believed to be existed between 0.8Hz and 1.1Hz. Along with plots of gains across frequencies in each visual condition (Figure A-3), it suggests the gain of head acceleration increase significantly at 1.1Hz. And there is no significant difference of gains in terms of type of disease.



(a)



(b)

Figure A-3 gains of head across frequencies in each visual condition. Visual conditions included here: (a) EO
(b) EC

Phase analysis converted the phase of head acceleration relative to sled within the range from 90 to 450° in all experimental conditions. In results shown in Figure A-4, subjects respond the phase close to 360° in most conditions except the subject WB in conditions of 0.8EC and 1.1EC. Along with suggestion from gain plots, phase results indicate heads of subjects were almost locked to sled.

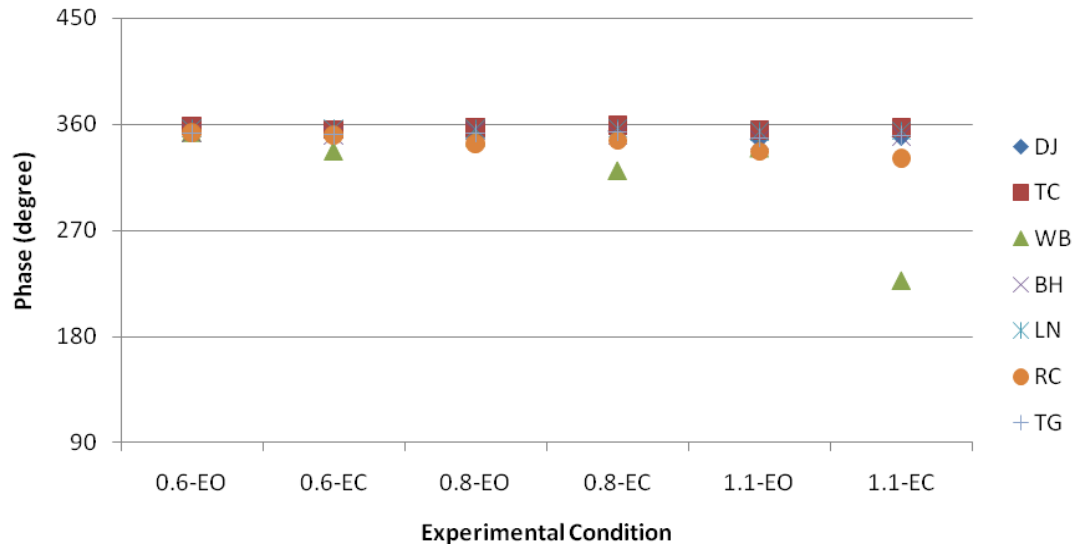


Figure A-4 phase of head acceleration relative to sled

APPENDIX B

ACCELERATION CONVERSION FACTOR

Each accelerometer was named as #number

#1 ADXL321EB-1

X direction: $G=18.23V-26.13$ (5V-5V module)

Y direction: $G=18.51V-26.66$ (5V-5V module)

#2 ADXL320EB

X direction: $G=5.712V-8.531$ (No module)

Y direction: $G=5.549V-8.306$ (No module)

#3 ADXL321EB-2

X direction: $G=74.04V-25.38$ (20V-5V module)

Y direction; $G=71.42V-25.64$ (20V-5V module)

#4 EVAL-ADXL335Z -1

X direction: $G=2.856V-5.303$ (1V-5V module)

Y direction: $G=14.18V-5.013$ (20V-5V module)

Z direction: $G=14.28V-5.142$ (20V-5V module)

#5 EVAL-ADXL335Z-2

X direction: $G=3.389V-4.869$ (5V-5V module)

Y direction: $G=2.777V-5$ (1V-5V module)

Z direction: $G=3.571V-5.178$ (5V-5V module)

#6 ADXL-320EB

X direction: $G=4.995V-8.909$ (1V-5V module)

Y direction: $G=5V-8.75$ (1V-5V module)

#7 ADXL-321EB-2

X direction: $G=13.31V-24.98$ (1V-5V module)

Y direction; $G=14.28V-26.71$ (1V-5V module)

APPENDIX C

MATLAB CODES FOR PROCESSING ACCLERATION DATA

Matlab codes basically include four function programs. The first three programs obtained raw data of acceleration from each channel and took it to fit a linear regression model. Fitted acceleration data with its amplitude, phase and offset, etc were exported and saved in EXCEL file sheets. Raw and fitted acceleration data were also plotted in Matlab figure. The fourth function program obtained the frequency response of fitted acceleration data.

```
1) function name_in = readdata_R(S)

num = [.1, .2, .5, 1.1];
str = ['SW', 'EO', 'EC', 'BW'];
col = ['B', 'C', 'D', 'E', 'F', 'G', 'H', 'I', 'J', ...
      'K', 'L', 'M', 'N', 'O', 'P', 'Q', 'R', 'S', 'T', 'U', 'V', 'W', 'X', 'Y', 'Z'];
mkdir(strcat('E:\results\',S));

procnum = 1;
for ii = 1:length(num)
    for jj = 1:4
        for kk = 1:3
            name1 = strcat('E:\Subject test\',S,'\ ',num2str(num(ii)),'-
',str(2*jj-1:2*jj),num2str(kk),'_RJ','.xls');
            data1 = xlsread(name1, 'sheet1', 'B2:I15000');
            % name_in = strcat('E:\Subject
test\',S,'\ ',num2str(num(ii)),'-',str(2*jj-1:2*jj),num2str(kk),'.lvm');
            % data = dlmread(name_in,'\t',22,0);
            disp(sprintf('process number = %d',procnum))
            procnum = procnum + 1;
            for nn = 1:8
                [t, g,p,off,pred,b]=fitsin(data1(:,nn),500,num(ii));
                name_out = strcat('E:\results\',S,'\ ',num2str(num(ii)),'-
',str(2*jj-1:2*jj),num2str(kk),'.xls');
                %columnHeader = {'','Accel-1-X','Accel-1-Z','Accel-1-
Y','Accel-2-X','Accel-3-X','Accel-4-Z','Accel-4-X','Accel-4-Y'};
                columnHeader =
{'','Sled_X','Trunk_X','Head_1_X','Head_1_Y','Head_1_Z','Head_4_X','Hea
d_4_Y','Head_4_Z'};
                rowHeader = {'','Amp.','Phase','Offset','R^2','F','p
value','estimate of the error variance'};
                xlswrite(name_out,columnHeader,'sheet1','A1');
                xlswrite(name_out,rowHeader,'sheet1','A1');
                xlswrite(name_out,g,1,strcat(col(nn),'2'));
                xlswrite(name_out,p,1,strcat(col(nn),'3'));
```

```

        xlswrite(name_out,off,1, strcat(col(nn), '4'));
        xlswrite(name_out,b,1, strcat(col(nn), '5'));
        xlswrite(name_out,columnHeader, 'sheet1', 'A10');
        xlswrite(name_out,pred,1, strcat(col(nn), '11'));
%starting from eleventh coloumn
        end
        xlswrite(name_out,t,1, 'A11');
%starting from eleventh coloumn
        end
    end
end

2) function [t,g,p,off,pred,b]=fitsin(y,SamplingRate,f)
% function [g,p,off,pred]=fitsin(y,f);
% fit sine wave with known frequency f to data vector y
% SamplingRate: sampling rate of vector y
% g: gain
% p: phase in degs
% off: offset
% pred: fitted sine wave
% stats: R^2, F, p as in REGRESS

if size(y,1)==1,
    y=y';
end
t=[0:length(y)-1]/SamplingRate;
if exist('regress')~=2,
    pars=[ones(length(y),1) sin(2*pi*f*t) cos(2*pi*f*t)]\y;
    stats=[0 0 0 0]*NaN;
else
    [pars,parsci,r,ri,stats]=regress(y,[ones(length(y),1) sin(2*pi*f*t)
cos(2*pi*f*t)]);
end
off=pars(1);
pred=pars(1)+pars(2)*sin(2*pi*f*t)+pars(3)*cos(2*pi*f*t);
g=sqrt(pars(2)^2+pars(3)^2);
p=atan2(pars(3),pars(2))*180/pi;
b=stats';

3) function readpitch(S)
num = [.1, .2, .5, 1.1];
str = ['SW', 'EO', 'EC', 'BW'];
col = ['B', 'C', 'D', 'E', 'F', 'G', 'H', 'I'];
dir = ['A-P head (F)';...
        'U-D head (F)';...
        'M-L head (F)';...
        'A-P Trunk  ';...
        'A-P Sled    ';...
        'U-D head (T)';...
        'A-P head (T)';...
        'M-L head (T)'];

```

```

Begin=1;
End=48;

m=Begin;
while m<=End
for ii = 1:length(num)
    for jj = 1:4
        for kk = 1:3

            name1 = strcat('E:\Subject test\',S,'\ ',num2str(num(ii)),'-
',str(2*jj-1:2*jj),num2str(kk),'_RJ','.xls');
            data1 = xlsread(name1, 'sheet1', 'A2:I15000');
            name2 = strcat('E:\results\',S,'\ ',num2str(num(ii)),'-
',str(2*jj-1:2*jj),num2str(kk),'_xls');
            data2 = xlsread(name2,1,['A11:I',num2str(length(data1))]);

            HeadX_F=data2(:,4)-mean(data2(:,4));
            HeadZ_F=data2(:,6)-mean(data2(:,6));
            HeadX_T=data2(:,7)-mean(data2(:,7));
            HeadZ_T=data2(:,9)-mean(data2(:,9));

            SledX=data2(:,2)-mean(data2(:,2));
            TrunkX=data2(:,3)-mean(data2(:,3));

            HeadPitch_F = sign(HeadX_F) .*sqrt(HeadX_F.^2 +
HeadZ_F.^2);
            HeadPitch_T = sign(HeadX_T) .*sqrt(HeadX_T.^2 +
HeadZ_T.^2);
            t=data2(:,1);
            L=length(t);
            Fs = 1/(t(2)-t(1));
            NFFT=2^nextpow2(L);
            f=Fs/2*linspace(0,1,NFFT/2);

            subplot(4,1,1)
            Y1=fft(HeadPitch_F,NFFT)/L;
            R1=max(2*abs(Y1(1:NFFT/2)));%maxium amplitude
            YY1=2*abs(Y1(1:NFFT/2));
            RR1= f(YY1==max(YY1));           % the corresponding frequency
            P1=angle(Y1(1:NFFT/2));
            PP1=P1(f==f(YY1==max(YY1)))*180/pi; % the corresponding phase
            plot(f,YY1,'linewidth',1.2);

            title('HeadPitch_F','FontSize',10)
            ylabel('Accel.(g)','FontSize',10)
            grid on
            set(gcf,'Position',[152 60 560 420])
            set(gca,'xlim',[0 10])

            subplot(4,1,2)
            Y2=fft(HeadPitch_T,NFFT)/L;
            R2=max(2*abs(Y2(1:NFFT/2)));%maxium amplitude
            YY2=2*abs(Y2(1:NFFT/2));

```

```

RR2= f(Y2==max(Y2));           % the corresponding frequency
P2=angle(Y2(1:NFFT/2));
PP2=P2(f==f(Y2==max(Y2)))*180/pi; % the corresponding phase
plot(f,Y2,'linewidth',1.2);

title('HeadPitch_T','FontSize',10)
ylabel('Accel.(g)','FontSize',10)
grid on
set(gcf,'Position',[152 60 560 420])
set(gca,'xlim',[0 10])

subplot(4,1,3)
Y3=fft(SledX,NFFT)/L;
R3=max(2*abs(Y3(1:NFFT/2))); %maxium amplitude
YY3=2*abs(Y3(1:NFFT/2));
RR3= f(YY3==max(YY3)); % the corresponding frequency
P3=angle(Y3(1:NFFT/2));
PP3=P3(f==f(YY3==max(YY3)))*180/pi; % the corresponding phase
plot(f,YY3,'linewidth',1.2);

title('SledX','FontSize',10)
ylabel('Accel.(g)','FontSize',10)
grid on
set(gcf,'Position',[152 60 560 420])
set(gca,'xlim',[0 10])

subplot(4,1,4)
Y4=fft(TrunkX,NFFT)/L;
R4=max(2*abs(Y4(1:NFFT/2))); %maxium amplitude
YY4=2*abs(Y4(1:NFFT/2));
RR4= f(YY4==max(YY4)); % the corresponding frequency
P4=angle(Y4(1:NFFT/2));
PP4=P4(f==f(YY4==max(YY4)))*180/pi; % the corresponding phase
plot(f,YY4,'linewidth',1.2);

title('TrunkX','FontSize',10)
xlabel('Frequency (Hz)','FontSize',10)
ylabel('Accel.(g)','FontSize',10)
grid on
set(gcf,'Position',[152 60 560 420])
set(gca,'xlim',[0 10])

d={ 'maxium
amplitude', 'Frequency', 'Phase',strcat(num2str(num(ii)),'-',str(2*jj-
1:2*jj),num2str(kk)); R1,RR1,PP1,NaN;...
R2,RR2,PP2,NaN; R3,RR3,PP3,NaN;R4,RR4,PP4,NaN};
name_out= strcat('E:\Subject test\',S,'\','freq.resp.','xls');
xlswrite(name_out,d,'Sheet1',[ 'A',int2str(5*m-4)]);
m=m+1;
saveas(gcf,strcat('E:\results\',S,'\','num2str(num(ii))','-',
',str(2*jj-1:2*jj),num2str(kk),'(PS-freq)','pdf'))
close

```

```

        end
    end
end
end

4) function plotthem3(S)
num = [.1, .2, .5, 1.1];
str = ['SW', 'EO', 'EC', 'BW'];
col = ['B', 'C', 'D', 'E', 'F', 'G', 'H', 'I'];
dir = [' headX(F)';...
      ' headZ(F)';...
      ' headY(F)';...
      ' TrunkX  ';...
      ' SledX   ';...
      ' headZ(T)';...
      ' headX(T)';...
      ' headY(T)'];

for ii = 1:length(num)
    for jj = 1:4
        for kk = 1:3
            name1 = strcat('E:\Subject test\',S,'\ ',num2str(num(ii)),'-
',str(2*jj-1:2*jj),num2str(kk),'.lvm');
            data1 = dlmread(name1,'\t',23,0);
            name2 = strcat('E:\results\',S,'\ ',num2str(num(ii)),'-
',str(2*jj-1:2*jj),num2str(kk),'.xls');
            data2 = xlsread(name2,1,['All:I',num2str(length(data1))]);
            figure

                for nn = 2:9
                    subplot(8,1,nn-1)
                    plot(data1(:,1),data1(:,nn),'r',
data2(:,1),data2(:,nn),'k')

                        m1 = max(data1(:,nn));
                        text(-4.5,m1/2, dir(nn-1,:), 'FontSize',9) %
                    end
                    xlabel('Time(s)')
                    legend('Experimental', 'Predicted', 'Location', 'NorthEast')
                    subplot 811
                    titlename=strcat(num2str(num(ii)),'-',str(2*jj-
1:2*jj),num2str(kk));
                    title(titlename)
                    saveas(gcf, strcat('E:\results\',S,'\ ',num2str(num(ii)),'-
',str(2*jj-1:2*jj),num2str(kk), '(KS-2)', '.pdf'))
                    close
                end
            end
        end
    end
end
end

```

APPENDIX D

RAW ACCELERATION DATA

The following tables list the data of the magnitude and phase of head acceleration based on fit-sine model from four subjects.

Table 6 Subject 1

Trial	Head (Frontal)		Sled		Gain	Phase
	Magnitude	Phase (0°/360°)	Magnitude	Phase (0°/360°)		
0.5-SW1	0.19	165.32	0.13	10.82	1.48	154.49
0.5-SW2	0.20	160.20	0.12	11.40	1.62	148.80
0.5-SW3	0.19	156.42	0.12	7.95	1.52	148.47
0.5-EO1	0.20	165.80	0.12	11.34	1.59	154.46
0.5-EO2	0.20	157.86	0.12	12.27	1.70	145.58
0.5-EO3	0.21	160.98	0.12	13.46	1.79	147.53
0.5-EC1	0.22	149.06	0.12	11.92	1.86	137.15
0.5-EC2	0.22	160.77	0.13	11.32	1.69	149.45
0.5-EC3	0.23	159.06	0.12	10.03	1.89	149.03
0.5-BW1	0.16	156.72	0.12	11.20	1.30	145.52
0.5-BW2	0.19	159.75	0.12	11.94	1.56	147.81
0.5-BW3	0.17	156.74	0.12	10.69	1.40	146.05
1.1-BW1	0.18	54.88	0.12	275.12	1.53	139.75
1.1-BW2	0.20	48.42	0.11	276.71	1.81	131.72
1.1-BW3	0.18	43.30	0.11	277.51	1.54	125.79
1.1-SW1	0.17	22.44	0.11	276.77	1.60	105.67
1.1-SW2	0.18	24.80	0.11	277.66	1.62	107.14
1.1-SW3	0.20	34.23	0.11	276.13	1.83	118.10
1.1-EO1	0.24	30.49	0.11	275.54	2.24	114.95
1.1-EO2	0.22	36.33	0.10	276.48	2.15	119.85
1.1-EO3	0.20	40.26	0.12	271.19	1.76	129.07
1.1-EC1	0.28	30.24	0.10	273.27	2.78	116.97
1.1-EC2	0.26	31.79	0.11	274.53	2.31	117.27
1.1-EC3	0.24	13.78	0.11	276.73	2.15	97.05
0.2-EO1	0.14	74.60	0.09	276.67	1.51	157.93
0.2-EO2	0.13	71.21	0.03	255.67	5.24	175.54
0.2-EO3	0.14	74.30	0.14	279.87	0.98	154.43
0.2-EC1	0.19	71.10	0.09	276.26	2.05	154.84

Table 5 Subject 1 (Continued)

0.2-EC2	0.20	75.97	0.15	276.95	1.33	159.03
0.2-EC3	0.18	72.32	0.08	277.48	2.14	154.84
0.2-BW1	0.19	79.86	0.09	282.69	2.00	157.17
0.2-BW2	0.15	86.85	0.02	264.40	7.52	182.44
0.2-BW3	0.16	81.44	0.07	275.75	2.17	165.69
0.2-SW1	0.13	82.85	0.04	267.60	3.31	175.26
0.2-SW2	0.13	81.00	0.08	278.44	1.62	162.56
0.2-SW3	0.15	87.13	0.14	278.27	1.04	168.87
0.1-EC1	0.07	197.27	0.06	43.49	1.23	153.77
0.1-EC2	0.08	197.12	0.04	37.19	1.98	159.93
0.1-EC3	0.08	212.90	0.08	44.89	0.95	168.01
0.1-BW1	0.09	214.60	0.05	39.47	1.74	175.13
0.1-BW2	0.07	224.64	0.06	39.15	1.18	185.49
0.1-BW3	0.09	229.33	0.07	42.38	1.41	186.95
0.1-SW1	0.06	252.87	0.02	35.94	2.47	216.93
0.1-SW2	0.06	189.29	0.05	39.76	1.20	149.53
0.1-SW3	0.06	213.70	0.05	40.04	1.23	173.65
0.1-EO1	0.07	179.15	0.03	38.63	2.34	140.53
0.1-EO2	0.11	185.65	0.05	39.95	2.18	145.70
0.1-EO3	0.08	194.23	0.05	39.10	1.70	155.13

Table 7 Subject 2

Trial	Head (Frontal)		Sled		Gain	Phase
	Magnitude	Phase (0°/360°)	Magnitude	Phase (0°/360°)		
0.2-EO1	0.11	29.15	0.09	277.45	1.28	111.70
0.2-EO2	0.13	53.29	0.07	273.20	1.88	140.09
0.2-EO3	0.15	55.94	0.07	273.57	2.01	142.37
0.2-EC1	0.15	52.77	0.10	277.09	1.46	135.68
0.2-EC2	0.18	49.57	0.09	275.01	2.04	134.56
0.2-EC3	0.16	44.58	0.11	276.75	1.44	127.82
0.2-BW1	0.12	57.98	0.10	277.05	1.15	140.93
0.2-BW2	0.11	53.36	0.10	278.10	1.11	135.27
0.2-BW3	0.15	55.48	0.09	275.91	1.63	139.58
0.2-SW1	0.13	65.04	0.11	277.07	1.12	147.97
0.2-SW2	0.13	60.02	0.10	276.25	1.26	143.77
0.2-SW3	0.15	63.84	0.10	279.22	1.45	144.61

Table 6 Subject 2 (Continued)

0.1-EC1	0.10	143.30	0.02	16.76	5.36	126.54
0.1-EC2	0.12	176.12	0.05	38.27	2.28	137.85
0.1-EC3	0.13	173.80	0.03	31.27	4.06	142.52
0.1-SW1	0.07	176.21	0.06	42.49	1.22	133.72
0.1-SW2	0.09	176.25	0.04	44.06	2.60	132.19
0.1-SW3	0.12	164.05	0.04	39.16	2.90	124.89
0.1-BW1	0.08	170.44	0.05	30.69	1.55	139.75
0.1-BW2	0.06	305.72	0.05	41.66	1.05	264.06
0.1-BW3	0.08	159.63	0.05	39.52	1.69	120.11
0.1-EO1	0.07	170.02	0.05	28.68	1.56	141.34
0.1-EO2	0.07	167.58	0.02	23.14	3.07	144.43
0.1-EO3	0.07	179.21	0.06	44.29	1.25	134.91
0.5-SW1	0.18	167.05	0.13	14.15	1.42	152.90
0.5-SW2	0.18	157.18	0.13	10.88	1.39	146.31
0.5-SW3	0.17	166.01	0.12	8.06	1.43	157.95
0.5-EO1	0.15	162.81	0.13	9.46	1.18	153.35
0.5-EO2	0.16	164.86	0.11	14.68	1.50	150.17
0.5-EO3	0.15	165.05	0.13	10.05	1.22	155.00
0.5-EC1	0.17	154.61	0.12	10.01	1.38	144.60
0.5-EC2	0.16	153.51	0.13	9.24	1.24	144.27
0.5-EC3	0.18	151.08	0.13	14.26	1.36	136.82
0.5-BW1	0.13	164.36	0.11	11.01	1.17	153.35
0.5-BW2	0.14	150.04	0.12	11.72	1.12	138.32
0.5-BW3	0.14	150.38	0.12	10.96	1.14	139.42
1.1-BW1	0.15	56.86	0.12	280.03	1.28	136.83
1.1-BW2	0.14	37.30	0.12	277.38	1.22	119.93
1.1-BW3	0.14	25.98	0.11	280.96	1.21	105.01
1.1-SW1	0.14	43.39	0.11	280.33	1.21	123.06
1.1-SW2	0.14	41.78	0.11	281.04	1.23	120.74
1.1-SW3	0.12	35.28	0.11	279.10	1.09	116.18
1.1-EC1	0.13	28.77	0.11	280.53	1.21	108.24
1.1-EC2	0.15	26.98	0.11	280.63	1.30	106.35
1.1-EC3	0.14	20.73	0.11	280.65	1.29	100.08
1.1-EO1	0.13	40.00	0.11	280.86	1.12	119.14
1.1-EO2	0.14	34.36	0.11	280.67	1.24	113.69
1.1-EO3	0.11	8.96	0.11	280.58	0.96	88.38

Table 8 Subject 3

trial	Head (Frontal)		Sled		Gain	Phase
	Magnitude	Phase (0°/360°)	Magnitude	Phase (0°/360°)		
0.1-EC1	0.05	210.26	0.05	217.92	1.09	352.33
0.1-EC2	0.04	222.57	0.05	220.80	0.88	1.77
0.1-EC3	0.05	210.08	0.05	219.98	0.99	350.10
0.1-BW1	0.05	228.52	0.05	220.24	0.98	8.28
0.1-BW2	0.05	222.01	0.05	222.09	1.05	359.91
0.1-BW3	0.05	219.79	0.05	218.96	1.13	0.83
0.1-SW1	0.04	213.42	0.05	220.45	0.94	352.97
0.1-SW2	0.05	214.24	0.05	221.39	1.00	352.84
0.1-SW3	0.05	224.64	0.05	220.57	1.14	4.07
0.1-EO1	0.04	231.71	0.05	219.71	0.89	12.00
0.1-EO2	0.04	236.73	0.05	220.80	0.90	15.92
0.1-EO3	0.05	223.65	0.05	219.35	0.95	4.31
0.2-EO1	0.11	95.20	0.09	96.76	1.27	358.44
0.2-EO2	0.10	92.56	0.09	96.67	1.15	355.89
0.2-EO3	0.10	96.44	0.09	96.89	1.12	359.55
0.2-EC1	0.11	78.28	0.09	97.33	1.22	340.95
0.2-EC2	0.10	90.30	0.09	95.86	1.18	354.44
0.2-EC3	0.10	81.64	0.09	96.51	1.08	345.12
0.2-BW1	0.11	89.34	0.09	97.35	1.21	351.99
0.2-BW2	0.10	91.58	0.09	96.35	1.20	355.23
0.2-BW3	0.10	90.31	0.09	96.93	1.15	353.37
0.2-SW1	0.11	92.22	0.09	96.98	1.25	355.24
0.2-SW2	0.10	97.95	0.09	97.41	1.16	0.53
0.2-SW3	0.09	97.82	0.09	97.37	1.05	0.45
1.1-EO1	0.19	60.09	0.11	99.08	1.78	321.01
1.1-EO2	0.18	65.87	0.11	99.71	1.73	326.15
1.1-EO3	0.17	60.28	0.11	100.09	1.59	320.19
1.1-SW1	0.16	64.19	0.11	99.97	1.55	324.22
1.1-SW2	0.16	60.77	0.11	99.79	1.52	320.99
1.1-SW3	0.16	60.85	0.11	99.65	1.46	321.20
1.1-EC1	0.17	45.18	0.11	99.98	1.60	305.20
1.1-EC2	0.17	52.50	0.11	99.76	1.58	312.74
1.1-EC3	0.18	47.50	0.11	100.11	1.73	307.40
1.1-BW1	0.15	52.37	0.11	99.75	1.39	312.62
1.1-BW2	0.15	62.00	0.11	99.94	1.40	322.06
1.1-BW3	0.14	62.72	0.11	99.92	1.34	322.80

Table 7 Subject 3 (Continued)

0.5-BW1	0.19	178.98	0.12	192.16	1.61	346.82
0.5-BW2	0.18	176.23	0.12	192.34	1.54	343.89
0.5-BW3	0.17	178.20	0.12	192.63	1.46	345.57
0.5-EC1	0.17	169.92	0.12	191.91	1.44	338.02
0.5-EC2	0.18	173.07	0.12	191.87	1.51	341.20
0.5-EC3	0.16	174.72	0.12	192.23	1.33	342.50
0.5-EO1	0.16	178.99	0.12	192.38	1.32	346.61
0.5-EO2	0.15	180.05	0.12	192.40	1.32	347.66
0.5-EO3	0.14	178.69	0.12	192.27	1.21	346.43
0.5-SW1	0.18	176.38	0.12	192.27	1.51	344.12
0.5-SW2	0.17	181.76	0.12	192.47	1.44	349.29
0.5-SW3	0.15	181.55	0.12	192.20	1.29	349.35

Table 9 Subject 4

	Head (Frontal)		Sled			
trial	Magnitude	Phase (0°/360°)	Magnitude	Phase (0°/360°)	Gain	Phase
0.1-EO1	0.06	210.41	0.05	220.24	1.26	350.17
0.1-EO2	0.05	218.74	0.05	221.80	1.04	356.94
0.1-EO3	0.06	208.01	0.05	224.76	1.35	343.25
0.1-EC1	0.07	201.66	0.04	221.33	1.53	340.32
0.1-EC2	0.06	203.51	0.05	222.62	1.40	340.89
0.1-EC3	0.06	213.59	0.05	221.69	1.38	351.90
0.1-BW1	0.07	193.72	0.05	220.02	1.39	333.71
0.1-BW2	0.06	196.91	0.05	219.14	1.34	337.76
0.1-BW3	0.06	201.77	0.05	226.73	1.34	335.04
0.1-SW1	0.06	213.40	0.05	223.62	1.12	349.78
0.1-SW2	0.05	211.24	0.05	219.61	1.17	351.63
0.1-SW3	0.06	224.09	0.05	219.40	1.21	4.70
0.2-SW1	0.12	78.01	0.09	96.54	1.38	341.47
0.2-SW2	0.12	80.64	0.09	98.42	1.39	342.22
0.2-SW3	0.12	87.28	0.09	95.52	1.31	351.76
0.2-EO1	0.12	88.79	0.09	97.56	1.39	351.23
0.2-EO2	0.11	90.30	0.09	96.61	1.28	353.69
0.2-EO3	0.11	89.90	0.09	97.17	1.28	352.73
0.2-EC1	0.12	90.24	0.08	97.94	1.47	352.30
0.2-EC2	0.12	87.16	0.09	95.92	1.37	351.24

Table 8 Subject 4 (Continued)

0.2-EC3	0.12	88.62	0.09	97.75	1.36	350.87
0.2-BW1	0.12	75.86	0.09	96.15	1.43	339.71
0.2-BW2	0.12	81.50	0.09	96.27	1.36	345.23
0.2-BW3	0.10	81.70	0.09	97.43	1.16	344.27
0.5-BW1	0.15	164.94	0.12	192.16	1.24	332.79
0.5-BW2	0.14	174.99	0.12	192.05	1.21	342.94
0.5-BW3	0.13	178.13	0.12	192.00	1.08	346.13
0.5-SW1	0.14	174.10	0.12	192.50	1.15	341.60
0.5-SW2	0.14	172.00	0.12	192.26	1.14	339.74
0.5-SW3	0.14	173.25	0.12	192.00	1.16	341.24
0.5-EO1	0.14	173.04	0.12	191.92	1.17	341.12
0.5-EO2	0.14	174.09	0.12	191.69	1.16	342.40
0.5-EO3	0.15	171.95	0.12	192.24	1.23	339.71
0.5-EC1	0.14	169.30	0.12	192.23	1.20	337.07
0.5-EC2	0.15	171.80	0.12	192.21	1.22	339.58
0.5-EC3	0.15	166.48	0.12	192.05	1.26	334.43
1.1-EO1	0.15	70.54	0.11	99.08	1.38	331.45
1.1-EO2	0.15	59.35	0.11	98.64	1.36	320.71
1.1-EO3	0.14	60.16	0.11	98.41	1.27	321.74
1.1-SW1	0.14	63.59	0.11	97.92	1.31	325.68
1.1-SW2	0.13	66.37	0.11	98.49	1.19	327.88
1.1-SW3	0.15	53.26	0.11	98.91	1.39	314.36
1.1-BW1	0.14	64.50	0.11	98.69	1.29	325.81
1.1-BW2	0.13	69.45	0.11	98.50	1.20	330.95
1.1-BW3	0.11	62.26	0.11	98.47	1.04	323.79
1.1-EC1	0.16	42.69	0.11	98.97	1.50	303.72
1.1-EC2	0.15	51.77	0.11	98.93	1.36	312.84
1.1-EC3	0.16	50.57	0.11	98.56	1.51	312.01